ROMANIAN ACADEMY

ROMANIAN ASTRONOMICAL JOURNAL

Vol. 22, No. 2
2012

EDITURA ACADEMIEI ROMÂNE

ROMANIAN ACADEMY

ROMANIAN ASTRONOMICAL JOURNAL

The ROMANIAN ASTRONOMICAL JOURNAL appears twice a year. Orders from abroad (issues or subscriptions) should be sent to:

EDITURA ACADEMIEI ROMÂNE, Calea 13 Septembrie nr. 13, sector 5, 050711, Bucharest, Romania, Phone: +(4021) 318 81 46, +(4021) 318 81 06, Fax: +(4021) 318 24 44, E-mail: edacad@ear.ro, Web: www.ear.ro

ORION PRESS IMPEX 2000, P.O. Box 77-19, sector 3, Bucharest, Romania, Phone/Fax: +(4021) 610 67 65, +(4021) 210 67 87; Tel.: 0311 044 668
E-mail: office@orionpress.ro

S.C. MANPRES DISTRIBUTION S.R.L., Piaţa Presei Libere nr. 1, Corp B, Etaj 3, Cam. 301–302, sector 1, Bucureşti
Tel.: 4021 314 63 39, fax: 4021 314 63 39
Email: abonamente@manpres.ro, office@manpres.ro
www.romanianjournals.com

The manuscripts, the books and journals proposed in exchange and the mail should be sent to the Editorial Board.

Editorial Board's Address:

ROMANIAN ASTRONOMICAL JOURNAL
Astronomical Institute of the Romanian Academy
Str. Cuţitul de Argint 5
RO-040557 Bucharest 28
Phone: +(4021) 335 68 92, +(4021) 335 80 10
Phone/Fax: +(4021) 337 33 89
E-mail: roaj@aira.astro.ro
http://www.astro.ro/~roaj/
Romania

ROMANIAN ASTRONOMICAL JOURNAL

Vol. 22 , No. 2, 2012

CONTENTS

GALAXY EVOLUTION IN THE ENVIRONMENT OF RDCS J1252.9-2927 AT $z \sim 1.24$ (II) - TANAKA CATALOG

NEDELIA ANTONIA POPESCU

Astronomical Institute of Romanian Academy
Str. Cutitul de Argint 5, 40557 Bucharest, Romania
Email: nedelia@aira.astro.ro

Abstract. In this paper we study the environment of RDCS J1252.9-2927, at $z = 1.237$, using the catalog of Tanaka *et al.*(2009) with optical-NIR photometric data and redshifts for 120 galaxies. The data from this catalog cover a wide field of 875 arcmin^2 (25 arcmin × 35 arcmin field), making possible the study of the large-scale structures in the field of RDCS J1252.9-2927 cluster. The color-color and color-magnitude diagrams of the galaxies that belong to the large-scale structures CLUMP 1 and CLUMP 2 in the RDCS J1252.9-2927 environment are presented. A large population of Extremely Red Galaxies (ERGs) in the studied sample of galaxies is determined. The photometric properties of galaxies in pairs and groups in the CLUMP 1 and CLUMP 2 are also analyzed.

Key words: galaxy groups and clusters - galaxy-galaxy interactions - galaxy pairs.

1. INTRODUCTION

The RDCS J1252.9-2927 cluster is one of the highest redshift X-ray clusters that was discovered in ROSAT Deep Cluster Survey (Rosati *et al.*, 2004). In the cosmological model $H_0 = 70$ km s^{-1} Mpc^{-1},$\Omega_m = 0.3$, $\Omega_\Lambda = 0.7$, $h = 0.7$, the total mass of the cluster inside 0.5 Mpc radius was estimated by Rosati *et al.* (2004) as being $M(< 0.5Mpc) = (1.9 \pm 0.3) \times M_\odot^{14}$.

In the same cosmological model, Lombardi *et al.* (2005) determined the total mass inside 1 Mpc radius to be $M(< 1Mpc) = (8 \pm 0.3) \times M_\odot^{14}$.

Blakeslee *et al.* (2003) reported the images obtained with the Advanced Camera for Surveys (ACS) on the Hubble Space Telescope (HST) in the F775W and F850LP bandpasses. A tight colour-magnitude relation (CMR) of early-type galaxies belonging to this cluster was revealed by these authors. In the core of the cluster a central pair of galaxies, with signs of dynamical interaction, surrounded by a large early-type galaxy population were determined due to the special resolution of ACS.

Lidman *et al.* (2004), Toft *et al.* (2004), and Strazzullo *et al.* (2006) obtained the ground-based near-IR imaging of RDCS J1252.9-2927 environment, underlying a clear near-IR color-magnitude relation (CMR). The luminosity function of the cluster galaxies was analyzed too, and a shallower slope than the value measured at similar

restframe wavelength in clusters in the local universe was revealed.

Due to a detailed dynamical and spectrophotometric information on galaxies in RDCS J1252.9-2927 high redshift cluster, Demarco *et al.* (2007) provided an in-depth view of structure formation at this epoch.

Tanaka *et al.* (2009) extended the investigation, obtaining wide-field imaging observations of the X-ray luminous cluster RDCS J1252.9-2927. Several galaxy groups that seem to be embedded in a filamentary structure extending from the cluster core are present inside the cluster.

Using GMOS on Gemini-South and FORS2 on VLT, Tanaka *et al.* (2009) performed a spectroscopic study of the galaxies in order to determine if these galaxies are physically associated to the cluster. The authors concluded that three groups contain galaxies at the cluster redshift, being probably bound to the cluster. The presence of such a filamentary structure as traced by galaxy groups at $z > 1$ was for the first time confirmed.

In the previous paper (Popescu, 2011) we combined the catalog of Demarco *et al.* (2007), that contains optical-NIR photometric data, redshifts, and morphology for galaxies (in a 36 arcmin^2 field), with Hubble Space Telescope/ Advanced Camera for Surveys archival images (from Hubble Space Telescope Archive at Canadian Astronomy Data Centre). The distribution of galaxies in the field of RDCS J1252.9-2927, taking into account their spectroscopic redshifts and morphology was analyzed. The role of color-color and color-magnitude diagrams in the characterization of Extremely Red Objects (EROs) was underlined. The photometric and morphological properties of galaxies in pairs and groups in the RDCS J1252.9-2927 environment were also determined. We especially consider the role of galaxy-galaxy interactions in triggering the star formation, and strong modification of galaxy morphologies and colors.

In this paper we study the environment of RDCS J1252.9-2927, at $z = 1.237$, using the catalog of Tanaka *et al.* (2009) with optical-NIR photometric data and redshifts for 120 galaxies.

The data from this catalog cover a large field of 875 arcmin^2 (25 arcmin $\times$ 35 arcmin field), making possible the study of the large-scale structures in the field of RDCS J1252.9-2927.

The color-color and color-magnitude diagrams of the galaxies that belong to the large-scale structures CLUMP 1 and CLUMP 2 in the RDCS J1252.9-2927 environment are presented. The photometric properties of galaxies in pairs and groups in the CLUMP 1 and CLUMP 2 are also analyzed.

2. DISTRIBUTION OF GALAXIES - TANAKA CATALOG

In the cosmological model $H_0 = 70$ km s^{-1} Mpc^{-1},$\Omega_m = 0.3$, and $\Omega_\Lambda = 0.7$, at the cluster redshift of $z = 1.237$, a linear size of 0.5 Mpc corresponds to $1'$ on the sky (*i.e.* $1''$ on the sky corresponds to 8.33 kpc in a physical distance).

Fig.1 presents the 2D distribution of galaxies in the RDCS J1252.9-2927 field for:

- the catalog of Demarco *et al.* (2007), with (B, V, R, $i775$, $z850$, K) optical-NIR photometric data, redshifts, and morphology for 38 confirmed cluster galaxies and redshifts for 189 field galaxies (in a 36 arcmin^2 field)- see Popescu (2011);

- the catalog of Tanaka *et al.* (2009), with (V, R, i', z', Ks) optical-NIR photometric data and redshifts for 120 galaxies positioned in CLUMP 1, CLUMP 2, CLUMP 3 and CLUMP 4 (in a 875 arcmin^2 field).

In both catalogs the magnitudes are on the AB system (Oke, 1974), being corrected for Galactic extinction.

Tanaka *et al.* (2007) observed RDCS J1252.9-2927 with Suprime-Cam (Miyazaki *et al.* , 2002) on the Subaru Telescope in the (V, R, i', z') bands, and K-band imaging with WFCAM on UKIRT (Henry *et al.* , 2000) and K_s-band imaging with SOFI on the ESO NTT (Moorwood, Cuby, and Lidman, 1998). In Tanaka *et al.* (2007) were for the first time presented four poor groups around the RDCS J1252.9-2927 cluster at $z \sim 1.24$.

In order to obtain spectroscopic follow-up observations of the structures discovered in Tanaka *et al.* (2007), Tanaka *et al.* (2009) used GMOS on Gemini-South (Hook *et al.* , 2004) and FORS2 on VLT UT1 (Appenzeller *et al.* , 1998). The catalog obtained by Tanaka *et al.* (2009) contains 102 objects with secure redshifts and 18 objects with possible redshifts.

In Fig.1, the RDCS J1252.9-2927 cluster can be clearly identified at the centre of the field, containing 38 confirmed cluster galaxies (big dots) and 189 field galaxies (small dots). In this figure North is up and Est is to the right. The distribution of $z \sim 1.24$ galaxies presents clumpy structures that surround the central main cluster. It can be observed the presence of a chain of clumps towards the N-NE direction from the cluster RDCS J1252.9-2927, reprezented by the CLUMP 1 and CLUMP 2, and extending over 15 Mpc transverse comoving distance. At the E-NE and W-SW of the main cluster a few more clumps are present. The CLUMP 3 and CLUMP 4 are located at E-NE of the main cluster, and W-SW of the main cluster, respectively. A large filamentary structure extending about 20 Mpc transverse comoving distance in the NE-SW direction is present.

The 3D distribution of the galaxies in the RDCS J1252.9-2927 cluster field function of the position (X,Y) and the spectroscopic redshifts z is presented in Fig.2.

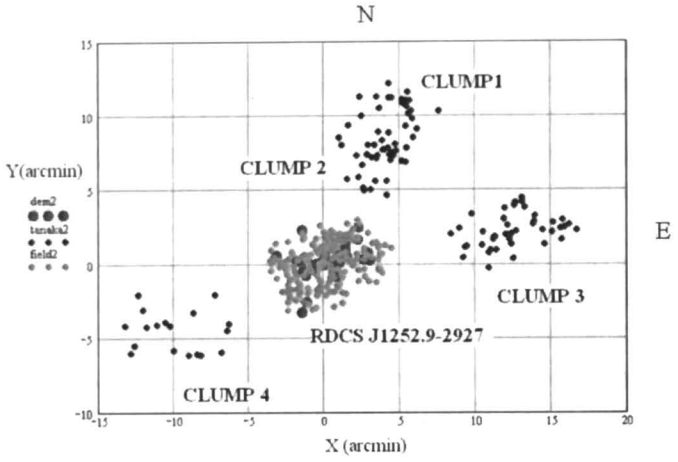

Fig. 1 – The 2D distribution of the galaxies in the RDCS J1252.9-2927 cluster field.

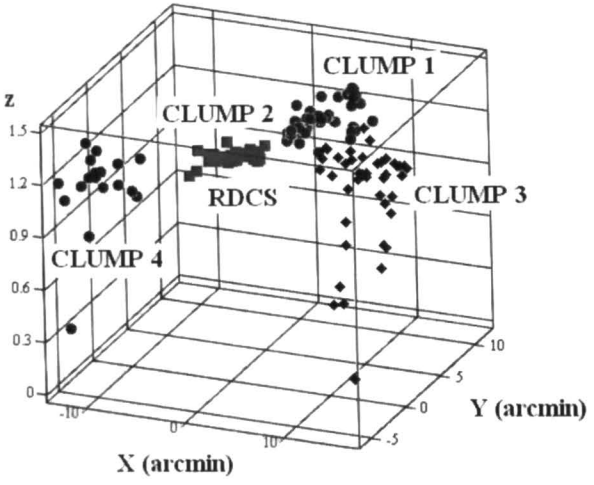

Fig. 2 – The 3D distribution of the galaxies in the RDCS J1252.9-2927 cluster field as function of the position (X,Y) and the spectroscopic redshifts z.

3. COLOR-MAGNITUDE AND COLOR-COLOR DIAGRAMS OF THE GALAXIES IN CLUMP 1 AND CLUMP 2

Elston *et al.* (1988) first discovered a special population denoted extremely red objects (EROs). These objects are characterized by very red optical and near-infrared colors, and are difficult to be classified due to their faintness. Extremely Red Galaxies (ERGs) are a subset of EROs, and are considered to be a mixture of mainly

two different populations at redshifts higher than $z = 1$.

The red colors of ERGs population are consistent with the following two classes of galaxies:

i) passively evolving early-type galaxies (elliptical and S0) in the redshift range $1 < z < 2$;

ii) high-redshift dusty starburst galaxies (characterized by high star-formation rates) whose UV luminosities are strongly absorbed by internal dust, or AGN reddened by strong dust extinction.

For the identification of galaxies clusters at $z \geq 1$, the selection criteria of the passively evolving elliptical galaxies by means of red optical and near-infrared colors have been usually used. Because the 4000 $\dot{A}$ break falls between R- (or I-, J-) band and K band, at $z \geq 1$ old passively-evolving galaxies should be characterized by red optical-NIR colors, which are redder than most galactic stars and field galaxies colors.

Both galaxy populations mentioned above satisfy color thresholds for ERGs such as $(R-K)_{Vega} \geq 5$, $(I-K)_{Vega} \geq 4$, $(V-I)_{Vega} \geq 3.5$, and have moderately faint near-infrared magnitudes ($K \sim 17.5-20$). These two populations can be separated by their morphology, spectra or color. Using the color-color diagrams, $(R-K)$ vs $(J-K)$ colors, Mannucci *et al.* (2002) have separated the two populations, and have found that the two populations have similar abundances in their 57 ERGs sample.

To analyze the ERGs in the Tanaka catalogue, we have to transform the photometry from the AB system to the Vega-based system using Fukugita, Shimasaku and Ichikawa (1995) transformations. The AB magnitudes and Vega-based magnitudes are denoted with (AB) and (Vega), respectively.

In our analysis the following transformation formulae from AB magnitudes to Vega-based magnitudes are considered:

$$V_{Vega} = V_{AB} - 0.011; R_{Vega} = R_{AB} - 0.199 \quad (1)$$

$$i'_{Vega} = i'_{AB} - 0.401; z'_{Vega} = z'_{AB} - 0.549 \quad (2)$$

For K magnitude the scales between the Vega-based magnitudes and the AB magnitudes are given by the formulae (Miyazaki *et al.* , 2003):

$$Ks_{Vega} = Ks_{AB} - 1.8 \quad (3)$$

$$(R-Ks)_{Vega} = (R-Ks)_{AB} + 1.6 \quad (4)$$

In this paper we define ERGs as objects whose color is equal to or redder than 3.4 (*i.e.* the condition $(R-Ks)_{AB} \geq 3.4$). This is the equivalent of the usual definition relation $(R-K)_{Vega} \geq 5$.

Because the goal of this paper is to analyze the ERGs distribution and the interactions effects on galaxies colors, in the sequel we analyze the color distribution of the galaxies that belong to CLUMP 1 and CLUMP 2 together (these two clumps being positioned very close to one another).

Fig.3 presents the 2D distribution of galaxies in CLUMP 1 and CLUMP 2, function of the spectroscopic redshifts z. From the 58 galaxies that belong to CLUMP 1 and CLUMP 2, in Fig.3 are represented 46 galaxies as follows: big dots - 18 galaxies with $z = 1.234$; diamonds - 5 galaxies with $z = 1.21$; (+) - 11 galaxies with $1.18 < z < 1.198$; small dots - 12 galaxies with $z = 1.1$. With big squares are marked the 15 galaxies that belong to the sample of galaxies pairs from CLUMP 1 and CLUMP 2.

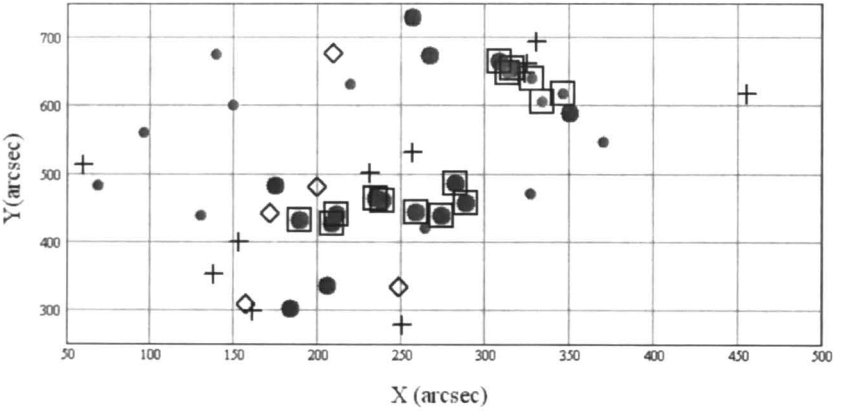

Fig. 3 – The 2D distribution of the galaxies in the CLUMP 1 and CLUMP 2 function of the spectroscopic redshifts z. The symbols are as follows: big dots - 18 galaxies with $z = 1.234$; diamonds - 5 galaxies with $z = 1.21$; (+) - 11 galaxies with $1.18 < z < 1.198$; small dots - 12 galaxies with $z = 1.1$.

The color-magnitude diagrams $(R-Ks)_{AB} - K_{AB}$, $(i'-Ks)_{AB} - K_{AB}$ and color-color diagram $(R-Ks)_{AB} - (i'-Ks)_{AB}$ of galaxies function of the spectroscopic redshifts z are presented in Fig.4. The symbols in Fig.4 are the same as in Fig.3. The dashed horizontal line in Fig.4 (top panel) represents the threshold $(R-Ks)_{AB} = 3.4$ for the selection of ERGs. In Fig.4 (middle panel) the two dashed horizontal lines represent the boundaries $(i'-Ks)_{AB} = 2.5$ and $(i'-Ks)_{AB} = 3.5$ for the galaxies in the red sequence. The vertical line represents the separation line between red and blue galaxies for $(i'-K)_{AB} = 2.5$, in Fig.4 (bottom panel).

The presence of a large population of ERGs in the CLUMP 1 and CLUMP 2 from the Catalog of Tanaka *et al.* (2009) is revealed by the color-color diagram

$(R-Ks)_{AB}-(i'-Ks)_{AB}$. The clustering of the 14 ERGs in specific colors ranges is obvious. The concentrations of red galaxies in the two clumps strongly suggest that these clumps are physically bound systems.

The color-color diagram $(V-i')_{AB}-(i'-z)_{AB}$, presented in Fig.5, is useful for the selection of Balmer/4000 $\dot{A}$ break galaxies and star-forming galaxies applying the selection criteria (Demarco *et al.* , 2007):

$$0.4 < (i'-z)_{AB} < 0.87; 0.2 < (V-i')_{AB} < 1.2 \quad (5)$$

$$2.4(i'-z)_{AB} - 1.12 < (V-i')_{AB} < 7(i'-z)_{AB} - 2.3 \quad (6)$$

The two population of old passive evolving galaxies and star-forming galaxies are well delimited in the $(R-Ks)_{AB}-(i'-Ks)_{AB}$ (Fig.4, bottom panel) and $(V-i')_{AB}-(i'-z)_{AB}$ (Fig.5) color-color diagrams. The red galaxies have colors in the specific range of the old passively evolving galaxies at $z \sim 1$. The condition $2.5 < (i'-Ks)_{AB} < 3.5$ is broad enough to include galaxies from the color-magnitude diagram in the red sequence. Also, the red sequence of studied galaxies is well delimited in the color-magnitude diagram $(R-Ks)_{AB}-Ks_{AB}$ from Fig.4 (top panel).

4. THE GALAXY PAIRS SAMPLE

To select kinematic galaxy pairs, in our study three steps are followed:

(1) For each galaxy in the spectroscopic redshift sample are determined the kinematic companions with a relative line-of-sight velocity difference $|\Delta v| \leq 500$ km s^{-1} and a projected physical separation (onto the plane of the sky) $r_{proj} \leq 300$ h^{-1} kpc.

(2) In the selected kinematic companions sample, close pairs are considered if they satisfy $10\ h^{-1}$ kpc $\leq r_{proj} \leq 50\ h^{-1}$ kpc (Lin *et al.* , 2007; Patton and Atfield 2008; Patton *et al.* , 2011).

(3) Wide pairs are identified as kinematic companions with $50\ h^{-1}$kpc $\leq r_p \leq 300\ h^{-1}$ kpc.

The linear distance between two galaxies can be obtained using the projected separation:

$$r_{proj} = \theta d_A(z_P). \quad (7)$$

The rest-frame relative velocity along the line of sight is determined as:

$$\Delta v = c|z_C - z_P|/(1+z_P). \quad (8)$$

In these formulae z_P is the redshift of the principal (more luminous) galaxy in the pair; z_C is the redshift of the companion galaxy; θ is the angular separation of the

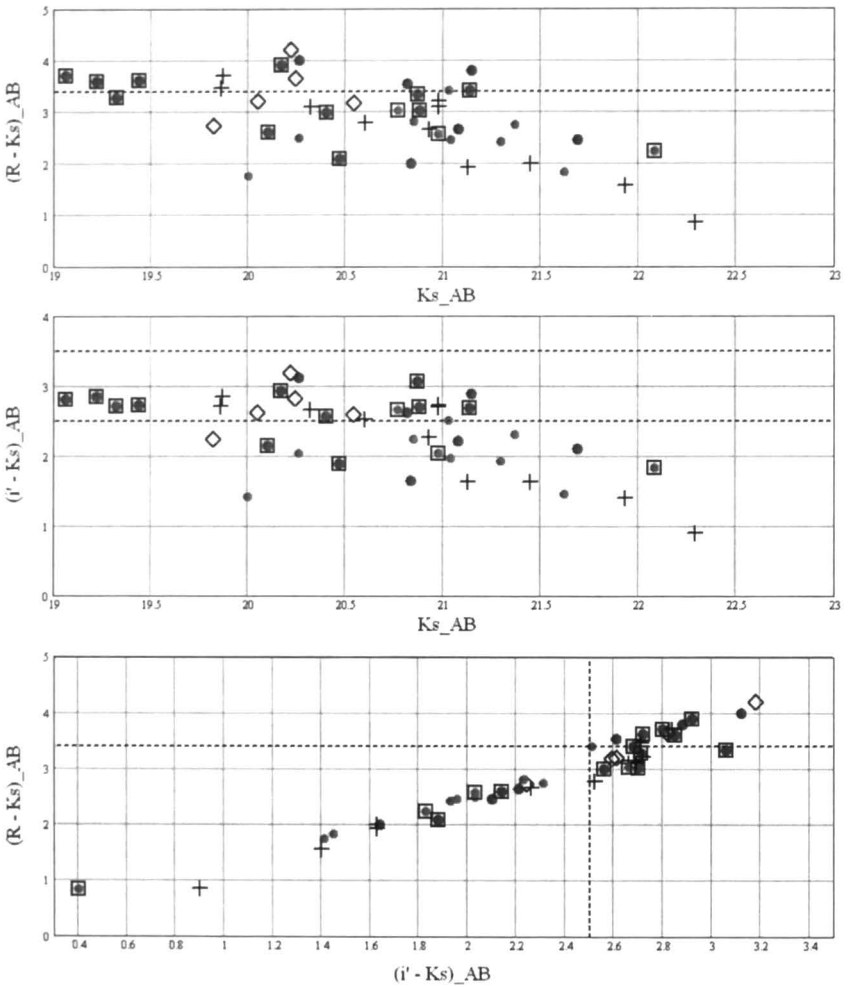

Fig. 4 – The $(R-Ks)_{AB}-Ks_{AB}$ color-magnitude diagram(top panel); $(i'-Ks)_{AB}-Ks_{AB}$ color-magnitude diagram (middle panel); $(R-Ks)_{AB}-(i'-Ks_{AB})$ color-color diagram (bottom panel); The symbols are as follows: big dots - 18 galaxies with $z\sim 1.234$; diamonds - 5 galaxies with $z=1.21$; (+) - 11 galaxies with $1.18<z<1.198$; small dots - 12 galaxies with $z=1.1$.

two galaxies on the sky plane (in arcsec); $d_A(z)$ is the angular scale at redshift z (in kpc/arcsec).

Because for the 46 galaxies in CLUMP 1 and CLUMP 2 secure redshifts are available, in the selection of our galaxy pairs sample we have the redshifts for both members of a pair. In this way the contamination due to unrelated foreground/ background companions is excluded, and we can compare intrinsic galaxy properties as a

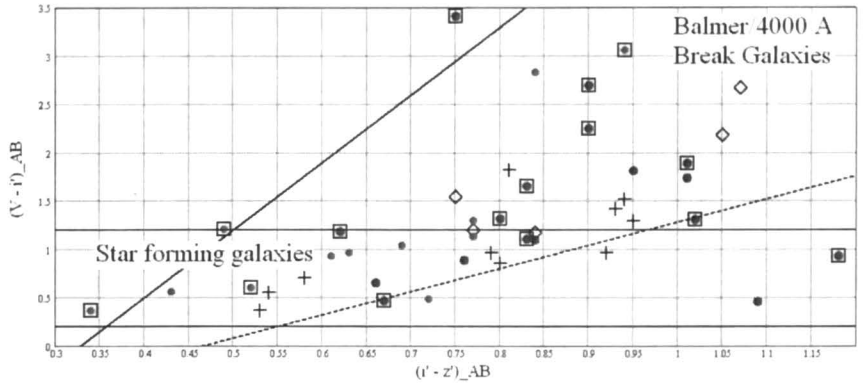

Fig. 5 – The $(V - i')_{AB} - (i' - z)_{AB}$ color-color diagram.

function of projected physical separation and relative line-of-sight velocity.

In Table 1 the photometric characteristics of the 15 galaxies in the galaxy pairs sample are described. We observe that the galaxies in pairs present obvious features of interactions, with bluer $(V - i')_{AB}$ and $(i' - z')_{AB}$ colors, as characteristics of interactions/mergers that trigger star formation activity.

Among the 15 galaxies that form 5 pairs and 2 triplets, only the pair formed by galaxies with identification number ID13 and ID15 has the projected distance less than 50 h^{-1}kpc, being a close pair of galaxies. The other galaxies represent wide pairs o galaxies, with projected distances in the range 100 h^{-1}kpc $\leq r_p \leq$ 270 h^{-1} kpc.

5. THE EFFECTS OF INTERACTIONS/MERGERS ON GALAXIES COLORS

Because of the different procedures for defining samples of galaxy pairs, the determined mergers present different properties.

Concluding, there are two main ways to define samples of mergers:

1) Based on morphological criteria - this procedure is focused on structural disturbances and/or tidal features (Bridge *et al.* , 2010; Chou *et al.* , 2011). Mergers tend to present strong morphological disturbances at the first encounter and the last merging stage. Then, the morphological selection criteria are biased toward selecting mergers at the final merging stages.

2) Based on a kinematic selection - this procedure identifies mergers by limiting the projected physical separation and the velocity differences between two close pair members (Patton *et al.* , 2000; Lin *et al.* , 2008; Patton and Atfield , 2008; Patton *et al.* , 2011).

In our study we used the kinematic selection in the detection of the galaxy

Table 1

The photometric characteristics of galaxy pairs sample

ID	K_{AB}	z_{spec}	$(R-Ks)_{AB}$	$(i'-Ks)_{AB}$	$(V-i')_{AB}$	$(i'-z')_{AB}$
5	19.06	1.235	3.70	2.80	2.70	0.90
6	20.17	1.237	3.90	2.92	2.25	0.90
19	20.88	1.234	3.02	2.70	3.41	0.75
17	20.87	1.226	3.34	3.06	0.93	1.18
22	21.14	1.231	3.41	2.68	1.31	1.02
13	20.40	1.231	2.99	2.56	1.11	0.83
15	19.32	1.235	3.29	2.71	1.32	0.80
18	19.22	1.233	3.60	2.85	1.89	1.01
21	20.10	1.234	2.60	2.14	1.18	0.62
14	19.44	1.235	3.62	2.72	1.65	0.83
14	19.44	1.235	3.62	2.72	1.65	0.83
47	20.47	1.231	2.09	1.88	0.47	0.67
2	22.08	1.068	2.23	1.83	0.60	0.52
1	24.63	1.071	0.83	0.40	0.37	0.34
8	20.77	1.070	3.03	2.66	3.06	0.94
9	20.98	1.070	2.57	2.03	1.21	0.49

mergers sample, as was presented in the previous section.

In order to investigate the interactions/mergers effects on galaxy colors, in Fig.6 the color-magnitude diagram $(R-Ks)_{AB}-K_{AB}$ and color-color diagram $(R-Ks)_{AB}-(i'-Ks)_{AB}$ for the 15 galaxies in pairs are presented.

In Fig.7 is displayed the color-color diagram $(V-i')_{AB}-(i'-z)_{AB}$ for the studied pairs of galaxies. This diagram is useful for the selection of Balmer/4000 $\dot{A}$ break galaxies and star-forming galaxies applying the selection criteria of Demarco *et al.* (2007).

In Figs. 6 and 7, the galaxies in pairs are represented with: big dots (ID5 and ID6 galaxies); diamonds (ID19, ID17, ID22 galaxies); crosses (ID13, ID15 galaxies); (X) (ID18, ID21, ID14 galaxies); squares (ID14, ID47 galaxies); small diamonds (ID1, ID2 galaxies); small dots (ID8, ID9 galaxies).

Clear evidences of interaction-induced star formation within the blue galaxies in pairs is revealed by Fig.7. Here a higher fraction of extremely blue galaxies are positioned in the *star forming galaxy region*. Also, the presence of red-red pair (candidate for dry merger), blue-blue pair (candidate for wet merger), and red-blue pair (candidate for mixed pair) in the determined sample of galaxy pairs can be observed in Fig.7. The wet mergers refer to galaxy mergers between gas-rich galaxies (*i.e.* mergers between galaxies with intense star formation), while dry mergers are those mergers between gas-poor galaxies (*i.e.* mergers between elliptical/spheroidal galaxies, that have weak star formation).

We classify as red fraction, the fraction of galaxies that either belong to the red

sequence or to the ERGs population (extremely red galaxies).

In the case of the galaxy pair sample from CLUMP 1 and CLUMP 2, one observes that the majority of blue-blue pairs are found in field-like environments. Also, red-red pairs and blue-red pairs tend to lie in denser environments (group and/or cluster-like environments), as can be seen from Fig.3 and Table 1 inspection.

The group of galaxies with $z \sim 1.24$ contains mainly red-red pairs and 3 mixed red-blue pairs, as can be observed from Table 1.

The only close pair of galaxy (ID13, ID15), with $r_p = 41.5$ kpc, belonging to the group of galaxies with $z \sim 1.24$, has the photometric characteristics:
- ID2 galaxy: K_{AB}=20.40, $(R-Ks)_{AB}$=2.99, $(i'-Ks)_{AB}$=2.56, $(V-i')_{AB}$=1.11, $(i'-z')_{AB}$= 0.83;
- ID1 galaxy: K_{AB}=19.32, $(R-Ks)_{AB}$=3.29, $(i'-Ks)_{AB}$=2.71, $(V-i')_{AB}$=1.32, $(i'-z')_{AB}$= 0.80.

The clump of galaxies with $z \sim 1.1$ contains only 2 galaxy pairs that present the most bluer colors in the sample. These pairs are positioned in a field-like environment.

The blue - blue pair (ID2, ID1) has a projected distance $r_p = 132$ kpc and the photometric characteristics:
- ID2 galaxy: K_{AB}=22.08, $(R-Ks)_{AB}$=2.23, $(i'-Ks)_{AB}$=1.83, $(V-i')_{AB}$=0.70, $(i'-z')_{AB}$= 0.52;
- ID1 galaxy: K_{AB}=24.63, $(R-Ks)_{AB}$=0.83, $(i'-Ks)_{AB}$=0.40, $(V-i')_{AB}$=0.37, $(i'-z')_{AB}$= 0.34.

This galaxy pair contains the faintest and bluest galaxies in the sample of 46 galaxies from CLUMP 1 and CLUMP 2.

The red - blue pair (ID8, ID9) has the photometric characteristics:
- ID8 galaxy: K_{AB}=20.77, $(R-Ks)_{AB}$=3.03, $(i'-Ks)_{AB}$=2.66, $(V-i')_{AB}$=3.06, $(i'-z')_{AB}$= 0.94;
- ID9 galaxy: K_{AB}=20.98, $(R-Ks)_{AB}$=2.57, $(i'-Ks)_{AB}$=2.03, $(V-i')_{AB}$=1.21, $(i'-z')_{AB}$= 0.49.

The wet and dry merging populations show different evolutionary trends. In their recent studies, Lin *et al.* (2008), De Propris *et al.* (2010), and Chou *et al.* (2011) show that the fraction of dry mergers (from the total merging galaxy population) is low at high redshifts (at $z > 0.5$), but becomes important at low redshifts ($z < 0.2$).

6. CONCLUSIONS

In this paper we study the environment of RDCS J1252.9-2927, at $z = 1.237$, using the catalog of Tanaka *et al.* (2009) with optical-NIR photometric data and

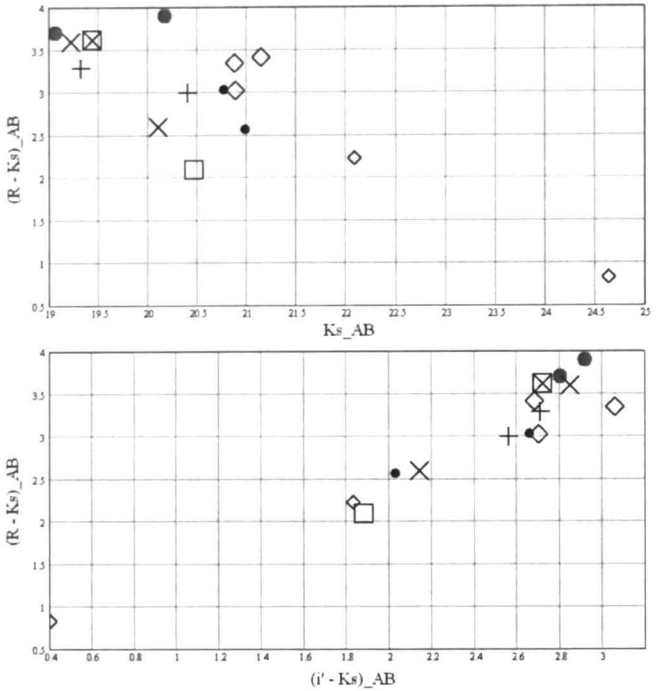

Fig. 6 – The $(R-Ks)_{AB} - Ks_{AB}$ color-magnitude diagram for the galaxy pair sample (top panel) and $(R-Ks)_{AB} - (i'-Ks_{AB})$ color-color diagram (bottom panel).
The symbols are as follows: big dots (ID5 and ID6 galaxies); diamonds (ID19, ID17, ID22 galaxies); crosses (ID13, ID15 galaxies); (X) (ID18, ID21, ID14 galaxies); squares (ID14, ID47 galaxies); small diamonds (ID1, ID2 galaxies); small dots (ID8, ID9 galaxies).

redshifts for 120 galaxies. The data from this catalog cover a wide field of 875 arcmin^2 (25 arcmin $\times$ 35 arcmin field).

In the field of RDCS J1252.9-2927, the distribution of galaxies presents 4 clumpy structures that surround the central main cluster. A large filamentary structure extending about ~ 20 Mpc in the NE-SW direction is present. Because of the concentrations of red galaxies in the clumps, it is strongly suggested that these are physically bound systems.

The color-color and color-magnitude diagrams of the galaxies that belong to the large-scale structures CLUMP 1 and CLUMP 2 in the RDCS J1252.9-2927 environment are presented. By means of these diagrams, a large population of 14 Extremely Red Galaxies (ERGs) is determined.

A strong pair isolation criterion in terms of the apparent angular separation and rest-frame line-of-sight velocity difference is used to obtain the galaxy pairs sample. The photometric properties of galaxies in pairs and triplets in CLUMP 1 and CLUMP

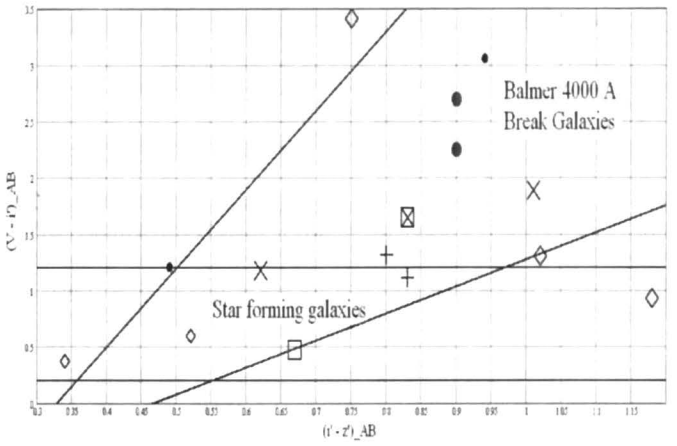

Fig. 7 – The $(V - i')_{AB} - (i' - z)_{AB}$ color-color diagram for the galaxy pair sample. The symbols are as follows: big dots (ID5 and ID6 galaxies); diamonds (ID19, ID17, ID22 galaxies); crosses (ID13, ID15 galaxies); (X) (ID18, ID21, ID14 galaxies); squares (ID14, ID47 galaxies); small diamonds (ID1, ID2 galaxies); small dots (ID8, ID9 galaxies).

2 are also analyzed. A large fraction of red galaxies in pairs or triplets is determined (11 red galaxies from the 15 galaxies in pairs). The redder colours are due to the higher densities of galaxies (especially for CLUMP 2) and the fact that galaxy colour and local density are correlated. The bluer optical-NIR colors of galaxies is a result of an increased star formation rate due to possible interactions/mergers.

REFERENCES

Appenzeller, I., Fricke, K., Fürtig, W., Gässler, W., Häfner, R., Harke, R., Hess, H.-J., Hummel, W., Jürgens, P., Kudritzki, R.-P., Mantel, K.-H., Meisl, W., Muschielok, B., Nicklas, H., Rupprecht, G., Seifert, W., Stahl, O., Szeifert, T., and Tarantik, K.: 1998, *The Messenger* **94**, 1.

Blakeslee, J.P., Franx, M., Postman, M., Rosati, P., Holden, B.P., Illingworth, G.D., Ford, H.C., Cross, N.J.G., Gronwall, C., Benítez, N., Bouwens, R.J., Broadhurst, T.J., Clampin, M., Demarco, R., Golimowski, D.A., Hartig, G.F., Infante, L., Martel, A.R., Miley, G.K., Menanteau, F., Meurer, G.R., Sirianni, M., and White, R.L.: 2003, *Astrophys. J.* **596**, L143.

Bridge, C.R., Carlberg, R.G., and Sullivan, M.: 2010, *Astrophys. J.* **709**, 1067.

Chou, R.C.Y., Bridge, C.R., and Abraham, R.G.: 2011, *Astron. J.* **141**, 87.

Demarco, R., Rosati, P., Lidman, C., Girardi, M., Nonino, M., Rettura, A., Strazzullo, V., van der Wel, A., Ford, H.C., Mainieri, V., Holden, B.P., Stanford, S.A., Blakeslee, J.P., Gobat, R., Postman, M., Tozzi, P., Overzier, R.A., Zirm, A.W., Benítez, N., Homeier, N.L., Illingworth, G.D., Infante, L., Jee, M.J., Mei, S., Menanteau, F., Motta, V., Zheng, W., Clampin, M., and Hartig, G.: 2007, *Astrophys. J.* **663**, 164.

De Propris, R., Driver, S.P., Colless, M., Drinkwater, M.J., Loveday, J., Ross, N.P., Bland-Hawthorn, J., York, D.G., and Pimbblet, K.: 2010, *Astron. J.* **139**, 794.

Fukugita, M., Shimasaku, K., and Ichikawa, T.: 1995, *Pub. Astron. Soc. Pac.* **107**, 945.

Henry, D.M., Atad-Ettedgui, E., Casali, M.M., Bennett, R.J., Bridger, A., Ives, D.J., Rae, R.G., and

Hawarden, T.G.: 2000, *Society of Photo-Optical Instrumentation Engineers (SPIE) Conference Series* **4008**, 1325.

Hook, I.M., Jørgensen, I., Allington-Smith, J.R., Davies, R.L., Metcalfe, N., Murowinski, R.G., and Crampton, D.: 2004, *Pub. Astron. Soc. Pac.* **116**, 425.

Lidman, C., Rosati, P., Demarco, R., Nonino, M., Mainieri, V., Stanford, S.A., and Toft, S.: 2004, *Astron. Astrophys.* **416**, 829.

Lin, L., Koo, D.C., Weiner, B.J., Chiueh, T., Coil, A.L., Lotz, J., Conselice, C.J., Willner, S.P., Smith, H.A., Guhathakurta, P., Huang, J.-S., Le Floc'h, E., Noeske, K.G., Willmer, C.N.A., Cooper, M.C., and Phillips, A.C.: 2007, *Astrophys. J.* **660**, L51.

Lin, L., Patton, D.R., Koo, D.C., Casteels, K., Conselice, C.J., Faber, S.M., Lotz, J., Willmer, C.N.A., Hsieh, B.C., Chiueh, T., Newman, J.A., Novak, G.S., Weiner, B.J., and Cooper, M.C.: 2008, *Astrophys. J.* **681**, 232.

Lombardi, M., Rosati, P., Blakeslee, J.P., Ettori, S., Demarco, R., Ford, H.C., Illingworth, G.D., Clampin, M., Hartig, G.F., Benítez, N., Broadhurst, T.J., Franx, M., Jee, M.J., Postman, M., and White, R.L.: 2005, *Astrophys. J.* **623**, 42.

Mannucci, F., Pozzetti, L., Thompson, D., Oliva, E., Baffa, C., Comoretto, G., Gennari, S., and Lisi, F.: 2002, *Mon. Not. Roy. Astron. Soc.* **329**, L57.

Miyazaki, S., Komiyama, Y., Sekiguchi, M., Okamura, S., Doi, M., Furusawa, H., Hamabe, M., Imi, K., Kimura, M., Nakata, F., Okada, N., Ouchi, M., Shimasaku, K., Yagi, M., and Yasuda, N.: 2002, *Pub. Astron. Soc. Japan* **54**, 833.

Miyazaki, M., Shimasaku, K., Kodama, T., Okamura, S., Furusawa, H., Ouchi, M., Nakata, F., Doi, M., Hamabe, M., Kimura, M., Komiyama, Y., Miyazaki, S., Nagashima, C., Nagata, T., Nagayama, T., Nakajima, Y., Nakaya, H., Pickles, A.J., Sato, S., Sekiguchi, K., Sekiguchi, M., Sugitani, K., Takata, T., Tamura, M., Yagi, M., and Yasuda, N.: 2003, *Pub. Astron. Soc. Japan* **55**, 1079.

Moorwood, A., Cuby, J.-G., and Lidman, C.: 1998, *The Messenger* **91**, 9.

Oke, J.B.: 1974, *Astrophys. J. Suppl.* **27**, 21.

Patton, D.R., Carlberg, R.G., Marzke, R.O., Pritchet, C.J., da Costa, L.N., and Pellegrini, P.S.: 2000, *Astrophys. J.* **536**, 153.

Patton, D.R., and Atfield, J.E.: 2008, *Astrophys. J.* **685**, 235.

Patton, D.R., Ellison, S.L., Simard, L., McConnachie, A.W., and Mendel, J.T.: 2011, *Mon. Not. Roy. Astron. Soc.* **412**, 591.

Popescu, N.A.: 2011, *Romanian Astron. J.* **21**, 3.

Rosati, P., Tozzi, P., Ettori, S., Mainieri, V., Demarco, R., Stanford, S.A., Lidman, C., Nonino, M., Borgani, S., Della Ceca, R., Eisenhardt, P., Holden, B.P., and Norman, C.: 2004, *Astron. J.* **127**, 230.

Strazzullo, V., Rosati, P., Stanford, S.A., Lidman, C., Nonino, M., Demarco, R., Eisenhardt, P.E., Ettori, S., Mainieri, V., and Toft, S.: 2006, *Astron. Astrophys.* **450**, 909.

Toft, S., Mainieri, V., Rosati, P., Lidman, C., Demarco, R., Nonino, M., and Stanford, S.A.: 2004, *Astron. Astrophys.* **422**, 29.

Tanaka, M., Kodama, T., Kajisawa, M., Bower, R., Demarco, R., Finoguenov, A., Lidman, C., and Rosati, P.: 2007, *Mon. Not. Roy. Astron. Soc.* **377**, 1206.

Tanaka, M., Lidman, C., Bower, R.G., Demarco, R., Finoguenov, A., Kodama, T., Nakata, F., and Rosati, P.: 2009, *Astron. Astrophys.* **507**, 671.

Received on 5 October 2012

BV PHOTOMETRY OF PROMINENT RS CANUM VENATICORUM STAR UX ARI (HD: 21242)

AJAZ AHMAD, MANZOOR A. MALIK, ABDUL WAHID

University of Kashmir, Srinagar-J&K, India-190006
ICSC, Hawal, Srinagar-J&K, India-190002
Email: ajazorama@gmail.com; mmalik@kashmiruniversity.ac.in; wahidphysics@gmail.com

Abstract. We present the results of BV photoelectric photometry observations of UX Ari RS CVn Star, obtained on 14 nights during the observing run January- February, 2006, using $14''$ telescope and SSP-3 Photometer. Comparison of light curves during the year 1972 by (Hall,1975), 1995-1996, 2001-2002 by Aarum and Henry (Aarum & Henry, 2003), and our observations 2006 clearly shows the amplitude variation of light on different time scales.

Key words: Photometry; RS CV_n; Period; Light Curve.

1. INTRODUCTION

RS Canum Venaticorm (RS CV_n) type stars are chromospherically active binary systems. The most accepted definition of RS CV_n binaries used is based on the classification criteria first formulated by Hall (1972; 1976) with some modifications made by Fakel *et al.*(1986). Apart from the classical RS CV_n binaries, originally defined by Hall (1976), there are several other classes of binaries containing at least one late-type star which can attain similarly high levels of activity (Hall, 1989). These include: short period and long period RS CVn binaries; close binary systems containing a white dwarf or sub-dwarf secondary; semi-detached (Algol) or detached binaries containing a late type subgiant as the secondary star and an early type companion as the primary star; and contact (W UM_a-type) binaries (Padmakar and Pandey, 1999).

RS CV_n stars are bright and interesting and can be observed with a simple photoelectric photometer or CCD camera on a small telescope with ease by astronomers. The term RS CV_n binary is used for a system which show presence of strong Ca II H & K, and H emission in the spectrum. Variable light curves arising primarily due to rotational modulation of the stellar light by large star spots on the surface of the cooler component. The binary usually consists of one hotter component of the spectral type F or G and Luminosity class V or IV. The secondary cooler companion is usually a subgiant or giant massive K-type star. Both stars typically lie well inside their Roche lobe. RS CVn binaries have been further classified into three subgroups

according to their orbital period:

(i) short period system ($P_{orb} \leq 1$ day);

(ii) classical RS CV$_n$ ($1 \leq P_{orb} \leq 14$ days);

(iii) long period system ($P_{orb} \geq 14$ days) (Barwey, 2005).

Discoveries of new RS CVn binaries, apart from enriching the existing samples, are important for understanding the underlying physical parameters like rotation, age, metalicity etc, which are involved in generating and sustaining strong chromospheric and coronal activity in them (Padmakar *et al.*, 1999).

2. UX ARIETIS

UX Ari (HD 21242) is a non-eclipsing type triple-lined system (Duemmler and Aarun, 2001) where the two main components constitute a doubled lined spectroscopic RS CV$_n$ binary system comprising a hot G5V primary and an active cool Ko IV secondary star (Carlos and Popper 1971). UX Ari is located at a distance of 50.2 pc, having Vmax = 6.5 with orbital period of 6.4378553d. The oldest photometric observations of UX Ari to be found in the literature are first presented by Hall *et al.*(1975). Their light curve had an amplitude $\Delta v \approx 0.1$ mag and a period of 6. 43791 d, determined spectroscopically by Carlos & Popper (1971). Since then, photometric observations have been presented by several authors (Hall, 1977; Zeilik *et al.*, 1982; Mohin and Raveendran, 1989; Strassmeir *et al.*, 1989; Nelson and Zeilik, 1990; Raveendran and Mohin, 1995; Rodono *et al.*, 1992; Padmakar and Pandey, 1996; Fabricius and Markarov, 2000) UX Ari HD 21242 has been assigned the variable star designation UX ARi by Kukarkin *et al.*(1973). After the detection by Hjellming and Blankenship (1973) of radio emission from AR Lacertae, itself an RS CV$_n$ type binary, Hall *et al.*(1975) suggested that UX Ari, is the brightest RS CVn- type binary except for HD 118216.

According to Gibson, Hjellming, and Owen (1975) UX Ari is the second most active radio star (after Algol) in terms of flux density. It is well established that the UX Ari light curve is rotationally modulated and displays wave like behavior, *i.e.*, the time of minimum light occurs at different orbital phase in different observing seasons. It is also generally accepted that the rotationally modulated brightness variations seen in UX Ari and other RS CV$_n$ stars are caused by extended, cool spots on the surface of cool primary component (Aarum and Henry, 2003) previously published photometry of UX Ari reveal an anti-correlation between the V magnitude and B-V color index *i.e.*, the UX Ari system becomes bluer as it become fainter (Zeilik *et al.*, 1982; Wacker *et al.*, 1986; Rodono *et al.*, 1992; Ulvas and Henry, 2003; Padmaker and Panday, 1999; Raveendran and Mohni, 1995). UX Ari also displays strong emission of Ca II H & K lines and phase dependent variable H emission, characteris-

tic of an active chromosphere and corona (Raveendran and Mohin 1995). Strong Ca II H & K emission is supposed to coming from cooler Ko star of the system (Fabricius and Markarov, 2000). The active cool star is also supposed to fill its Roche lobe and probably some mass transfer from the primary Ko star to the secondary G5 star is taking place (Huenemoerder, 1989). UX Ari displays strong radio flares. This star shows an intense coronal emission at x-ray wavelength, and hence it has been extensively studied since its discovery as an x-ray source using various X-ray observatories. Einstein slew survey (Schachter *et al.*, 1996) shows that UX Ari is rather an average x-ray luminous star having plasma temperature of $\simeq$ 107K. Further, chromospheric cycle of about 7 years has been obtained for Ux Ari (Buccino and Mauas, 2009).

3. OBSERVATIONS OF UX ARI USING 14″ REFLECTOR TELESCOPE

The BV photoelectric photometric observations of UX Ari were carried out during the observing run during the period January-February 2006. Because of rather unfavorable sky conditions we could observe this star for a total of 14 nights only. All the photometric data was obtained using celestron C-14 Schmidt-Cassegrin reflector telescope mounted at Inter University Centre for Astronomy and Astrophysics (IUCAA), Pune, India. The detector used in SSP3 photometer. The response of the B, V filters used closely matches the Johnson standard B, V, R & I response function.

Observations of UX Ari (HD 21242) were carried out by using differential photometry technique which is the magnitude difference between two stars: the chosen variable star and the standard star taken as the comparison star very close to each other in the sky. This technique has capability to measure very small variations in brightness of the star even under adverse sky conditions. To test the non-variability of the comparison star, another star called the check star which also fulfill the selection criteria for comparison star is used. Advantage of having a check star is to determine the accuracy of differential photometry observations for individual nights *i.e.*, standard deviation of differential magnitude and color between comparison and check star gives a measure of uncertainty associated with each observing night. Apart from errors introduced by atmospheric conditions, differential photometry can overcome typical instrumental errors, for example, arising from mismatch of the filter detector combination with standard system (Barwey, 2005; Henden and Kaitchuck, 1990).

In order to obtain accurate differential photometry, we used two nearby stars 62 Ari (G5 III) having visual magnitude: 5.55 as comparison star and Tyc 1796-1308-1 HIP 15548, HD 20644 (K211-111) having visual magnitude: 4.47 as check star. We followed the observing sequence for differential photometry during all observing nights as com S V Ch com S V Ch where com, V, Ch and S represents compari-

Table 1

Observational Data of Uxari Variable star in V- band

JD_V	Ph_V	ΔV	ΔV_c
2453754.087627	0.643276	1.111	1.0288
2453755.097951	0.800159	1.025	1.0543
2453756.177106	0.967915	0.739	1.0234
2453757.078055	0.10786	1.1370	1.0330
2453778.148969	0.27407	1.1841	0.6730
2453759.130370	0.426604	1.283	1.211
2453760.179305	0.589545	0.915	1.060
2453761.184837	0.745652	1.081	1.0235
2453762.133773	0.89306	1.045	0.999
2453763.175173	0.054914	1.127	1.077
2453764.135555	0.204031	1.182	1.0513
2453765.182303	0.366661	1.302	1.0091
2453768.209120	0.836845	1.202	1.0006
2453770.170925	0.141447	1.0870	1.188

son, variable, cheek stars and sky respectively. The observations were corrected for atmospheric extinction also.

The individual differential V observations are listed in table 1. The first column contains the Julian date. The second column contains the phase computed with the ephemeris:

$$JD = 2440133.^d76 + 6.^d43791E \quad (1)$$

For phase calculation we have taken fractional part of (JD-Epoch)/period. Where Epoch is the time of minimum light or JD at which minima of light curve occurs. Further the period is the variability period in days. From the ephemeris 2440133.76d is initial epoch, 6.43791 is the period and E is the cycle number (Ephemeris from Carlos & Popper, 1971). The third and fourth column contain the differential V magnitudes. Table 2 contains JD in the first column, phase calculation in the second column and last two columns contain the differential B magnitudes.

The graph of magnitude against time as in Fig.1 or against phase gives the light curve of UX Ari. The variability of UX Ari can be seen in Fig.1. Although we have only 14 nights of observation for this star but it is evident from the phase diagram (Fig.1) that the observations cover the entire phase. For comparison, along with our own observations, we plotted the light curve of UX Ari obtained from the data of Hall (1975) and from observations made by Aarum & Henry in year 1995-1996, 2001-2002 (Aarum & Henry, 2003) in Fig.4.

All the observations were corrected for differential atmospheric extinction using extinction coefficients Kb = 0.65 (Fig.2) for B- band and Kv = 0.43 (Fig.3) for V-band, obtained with the help of least square fitting method. Earlier photometry of

Table 2

Observational Data of UX Ari Variable Star in B band

JD_B	Ph_B	ΔB	ΔB_c
2453754.11125	0.6473003	0.713	0.669
2453755.104918	0.801246	0.713	0.665
2453756.192650	0.970245	0.832	0.634
2453757.087523	0.109265	1.0052	0.709
2453758.153148	0.274847	0.920	0.752
2453759.133576	0.427070	1.0007	0.663
2453760.193148	0.591720	0.915	0.658
2453761.193136	0.7475	0.828	0.713
2453762.137777	0.893681	0.768	0.711
2453763.178622	0.05538	0.887	0.611
2453764.138981	0.204496	0.943	1.182
2453765.188425	0.367593	1.0566	0.7143
2453768.212025	0.837311	0.867	0.781
2453770.175914	0.142223	0.9118	0.552

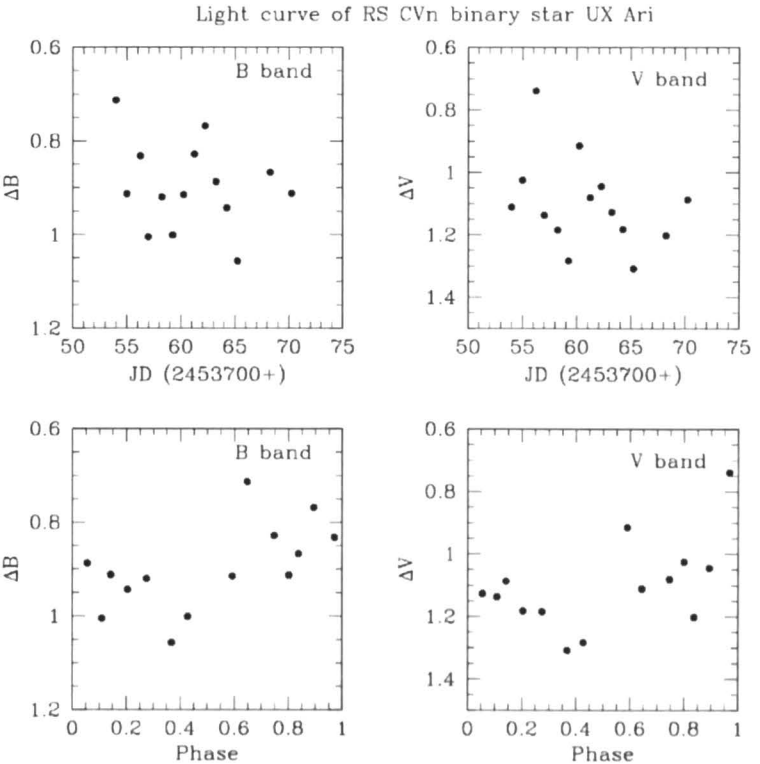

Fig. 1 – V band light curve and B band light curve.

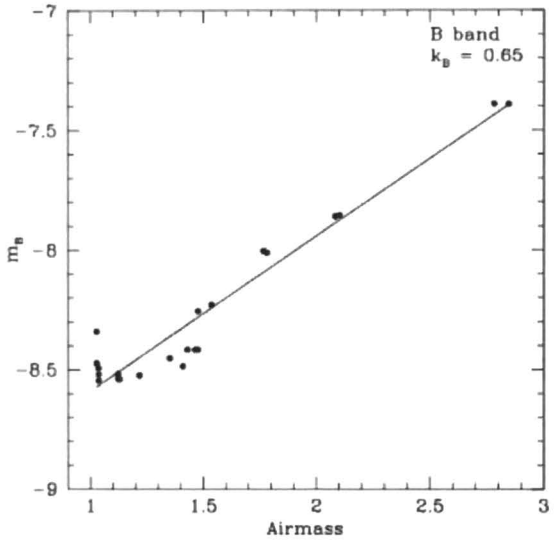

Fig. 2 – B- band extinction coefficient.

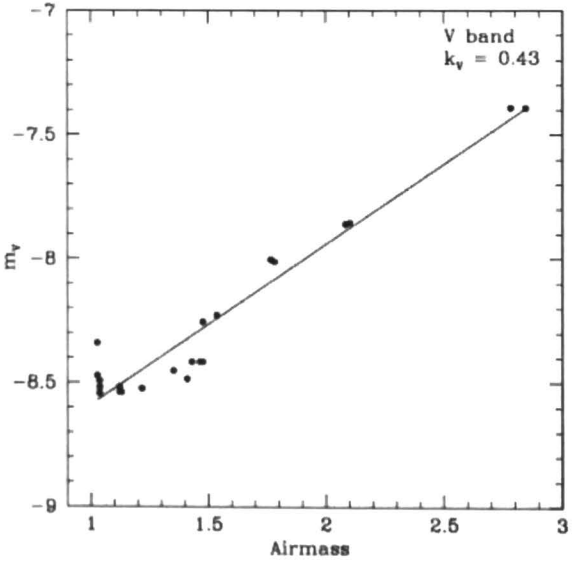

Fig. 3 – V- band extinction coefficient.

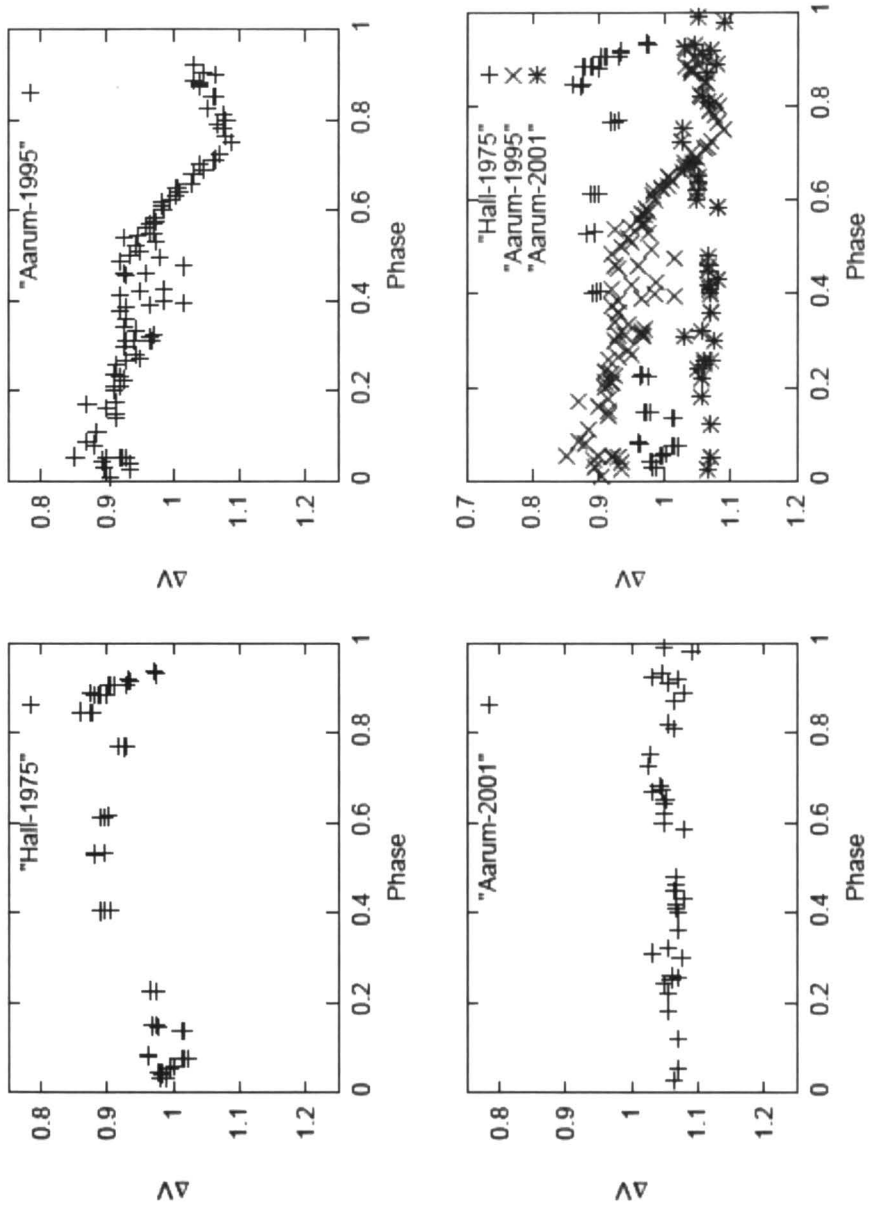

Fig. 4 – In this page, first three figures show light curves of Ux Ari for years 1975, 1995 and 2001. Fourth figure shows the the comparative study of light curves 1975, 1995, 2001.

UX Ari has shown its light to be variable on a variety of time scales (Fig.4)(Hall, 1975). There has been a nearly sinusoidal wave the amplitude of which has varied from year to year even within a year. Comparison of light curves during the year 1975 (Hall, 1975), 1995/1996; 2001/202 (Aarum and Henry 2003) in Fig.4 and our observations Jan-Feb 2006 (Fig.1) clearly shows the amplitude variation of light on different time scales.

4. CONCLUSIONS

In this paper we presented photometric observations and light curves of a prominent RS CVn Star Ux Ari (HD: 21242) and analysed them with published observations and light curves. The light curves obtained were analysed in B and V filters. These light curves are very similar to quasi-sinusoidal photometric curves commonly observed for various RS CVn Stars. Our main results are described below.

Although we observed this star only for 14 nights but it is evident from the phase diagram that observations cover the entire phase. For comparison, along with our observations we plotted the light curves from the published observations of (Hall *et al.*, 1975; Aarum and Henry, 2003).

All the observations were corrected for differential atmospheric extinction using extinction coefficients $K_b = 0.43$ for B-band shown in fig (2) and $K_v = 0.65$ for V-band shown in Fig.3.

Earlier photometry of Ux Ari (HD:21242) has shown its light to be variable on a variety of time scales and this change has been attributed due to the presence of large star spot activity. This variation in light can be clearly seen in Fig.4 obtained from observations of Hall et al.(1975) and observations of Aarum & Henry, 1995, 2001 (Aarum & Henry, 2003). Moreover, there has been a nearly sinusoidal wave amplitude of which has varied from year to year even within a year as can be observed from the light curves during the year 1995/1996, 2001/2002 from Fig.4 (Aarum and Henry, 2003). Our observations January- February 2006 in agreement with above clearly shows amplitude variation at different time scales, which is a good reason to believe that Ux Ari (HD: 21242) is a variable star.

REFERENCES

Aarum, V., Henry, G.W.: 2003, *Astron. Astrophys.* **402**, 1033.
Buccino, A.P., Mauas, P.J.D.: 2009, *Astron. Astrophys.* **495**, 287.
Barwey, S.: 2005, *PhD thesis.*
Carlos, R., Popper, D.M.: 1971, *PASP* **83**, 504.
Duemmler, R., Aarum, V.: 2001, *Astron. Astrophys.* **370**, 974.
Fabricius, C., Markarov, V.V.: 2000, *Astron. Astrophys.* **356**, 141.
Fakel, F.C., Moffet, J., Henry G.W.: 1986, *Astrophys. J.* **60**, 551.

Gibson, D.M., Hjellming, R.M., and Owen, F.N.: 1975, *Astrophys. J.* **200**, L99.
Hall, D.S.,: 1972, *PASP* **84**, 323.
Hall, D.S., Montle, R.E., Atkins, H.L.: 1975, *Acta Astron.* **25**, 125.
Hall, D.S.: 1976, *IAU Colloq.* **No. 29**.
Hall, D.S.: 1977, *Acta Astron.* **27**, 281.
Hall, D.S.: 1989, *SSRv.* **50**, 219H.
Henden, A.A; Kaitchuck, R.H.:1990, *Astronomical Photometry. Willman- Bell, Inc.*
Huenemoerder, D.P.: 1989, *Astron. J.* **98**, 2268.
HJellming, R.M., Blankenship, L.C.: 1973, *I.A.U. Circ.* **No. 2502**.
Kukarkin,*et al.*: 1973, *I.A.U Inf. Bull. Var.Stars* **No. 834**.
Landis., H.J.,*et al.*: 1978, *Astron. J.* **83**, 176.
Mohin, S., Raveendran, A.V.: 1989, *JA&AS* **10**, 35.
Nelson, E.R., Zelik, M.: 1990, *Astrophys. J.* **349**, 163.
Padmaker,*et al.*: 1999, *Astron. Astrophys. Suppl.* **138**, 203.
Padmakar, S.P., Pandey, S.K.: 1996, *Ap&SS* **235**, 337.
Padmakar, S.P., Pandey, S.K.: 1999, *Astron. Astrophys. Suppl.* **138**, 203.
Raveendran, A.V., Mohin, S.:1995, *Astron. Astrophys.* **301**, 788.
Raveendran, A.V., Mohin, S.: 1995, *Astron. Astrophys.* **301**, 788.
Rodono, M., Montle, Cutispoto,*et al.*: 1992, *Astron. Astrophys. Suppl.* **95**, 55.
Schachter, J.F.,*et al.*: 1996, *Astrophys. J.* **403**, 747.
Strassmeir, K.G.,*et al.*: 1989, *Astrophys. J. Suppl.* **69**, 141.
Wacker, S. W.,*et al.*: 1986, *IBVS* **2920**, 1.
Zeilik, M.,*et al.*: 1982, *Info. Bull. Var. Stars* **2168**, 1.

Received on 17 August 2012

EVOLUTION OF THE SOLAR WIND PLASMA PARAMETERS FLUCTUATIONS - ULYSSES OBSERVATIONS

NEDELIA ANTONIA POPESCU[1], EMIL POPESCU[2,1]

[1]*Astronomical Institute of Romanian Academy*
Str. Cutitul de Argint 5, 40557 Bucharest, Romania
Email: nedelia@aira.astro.ro
[2]*Technical University of Civil Engineering,*
Bd. Lacul Tei 124, 020396 Bucharest, Romania
Email: epopescu@utcb.ro

Abstract. The solar wind plasma parameters and interplanetary magnetic field fluctuations are studied for an interval of time that corresponds to Ulysses in-situ measurements of high-latitude heliospheric magnetic field, around the time of polarity reversal in 2001. Also the analyzed period in 2001 corresponds to the transition to the stationary fast flows, that starts from the day of the year (DOY) 240. Using data from Ulysses/ VHM instrument, the technique based on differencing of the original time series over a range of temporal scales have been considered for this study. The fluctuations of the magnetic field magnitude (B), and the corresponding RTN components (Br, Bt, Bn), at larger scales are less intermittent than at small scales. Their behaviour at different scales is quantitatively described by the probability distribution functions (PDFs) and generalized structure functions. Inside the studied interval of time, an ICME event can be observed between DOY 236.542 - DOY 237.042 of 2001, its signatures being also analyzed in this paper.

Key words: solar wind turbulence, solar wind plasma parameters fluctuations.

1. INTRODUCTION

Solar wind represents the continuous highly variable hot plasma that radially outflows from the Sun's corona, and moves at supersonic speeds, ranging from slightly below 300 km s^{-1} to about 2000 km s^{-1} during transient solar events. The magnetic field of the Sun, as well as different structures, waves and turbulent fluctuations on a wide range of scales are embedded within the solar wind.

The basic characteristic of the solar wind is represented by the two states of flow: fast streams and slow streams. These can be differentiated by kinetic parameters (speed, kinetic temperature), and more precisely by the elemental and charge state composition (see Feldman *et al.*, 2005). The compositional differences between the fast and slow solar wind appear because of their different origins in the corona.

From the first observations of the solar wind (Neugebauer and Snyder, 1962), it is known that the solar wind flows present variability on all timescales, that can be determined from the fluctuations of the solar wind plasma parameters and interplan-

etary magnetic field.

The intermittency in the solar wind is connected with the briskly occurrence, in space or time, of extreme events or large amplitude variations of plasma parameters, like the bulk velocity, or magnetic field magnitude.

In this paper we use statistical methods of analysis (probability distribution functions, and structure functions) for the investigation of solar wind plasma parameters and magnetic field intermittency.

We have to mention that the data provided by Ulysses for the year 2001 represent the first in-situ measurements of high-latitude heliospheric magnetic field around the time of polarity reversal. In 2001 around the DOY 236, at a heliolatitude of about 67° N, the last crossing of heliospheric current sheet was registered by Ulysses. Only the new northern polarity (inward polarity) was detected since that moment, with exceptionally short reversals during transient structures (Jones and Balogh, 2003).

Thus, the period studied in our work (between DOY 234 and DOY 238) represents a period of transition to the stationary fast flows (around 750 km s^{-1}), that starts from DOY 240 and lasts for a period of 100 days. For this long period only the high speed solar wind was observed at high heliolatitudes, Ulysses being positioned along the northern polar coronal hole.

Because 2000 - 2001 was a period of maximum solar activity, many extreme events were present such as transient ejections of solar material, the so-called coronal mass ejections (CMEs). Their interplanetary counterparts have been registered by Ulysses as interplanetary coronal mass ejections (ICMEs).

Such an ICME event can be observed between DOY 236.542 and 237.042 (Ebert *et al.*, 2009), its signatures being also analyzed in this paper. For our analysis we consider one-minute resolution data from VHM magnetometer instrument on board Ulysses spacecraft (for the magnetic field magnitude B), 4-minutes resolution data from SWOOPS/ Ulysses (for solar wind velocity V, density N, and temperature T), and 3 hour averaged data for temperature, plasma composition and charge-state measurements of solar wind ions from SWICS instrument. The analysis is realized for a period of 5 days, starting with the day of the year DOY 234 through DOY 238 of 2001.

In this paper we also present a detailed description and analysis of the ICME on 24 August 2001 by means of classical identification of ICMEs ($He++$ abundance enhancement, low kinetic temperature, low velocity); plasma dynamics signatures (thermal index $Ith > 1$); plasma composition signatures (anomalies of abundance and charge state of heavy ion species, low ion temperature and velocities).

2. SOLAR WIND PARAMETERS AND MAGNETIC FIELD DATA ANALYSIS

In this section we analyze the characteristics of the ICME event on DOY 236 (24 August 2001). During this event, Ulysses was situated above $67.5°N$, and at the heliocentric distances 1.75 AU.

The duration of the ICME on 24 August 2001 is 12 hours: between 24 August at 13:00 UT (DOY 236.542), and 25 August at 01:00 UT (DOY 237.042). In order to analyze the characteristic signatures of an ICME we consider the in situ data recorded by Ulysses with SWOOPS, VHM and SWICS instruments. This ICME presents the features of a magnetic cloud: the magnetic field rotates smoothly through a large angle, the strength of the magnetic field is higher than in the average solar wind, and the temperature is lower than that in the average solar wind (Burlaga *et al.*, 1981; Burlaga, 1991). Within the event time frame an average magnetic field magnitude of $< B >= 8.42 \pm 1.45$ (nT) and proton velocity of $< V >= 539 \pm 9$ km s^{-1} of the plasma are determined (Ebert *et al.*, 2009).

2.1. CLASSICAL SIGNATURES AND PLASMA DYNAMICS SIGNATURE DETECTION OF ICME

Interplanetary magnetic field data obtained from the Ulysses spacecraft during the passage of the ICME are presented in Fig.1. The time is expressed in day of the year (DOY). The one minute resolution data obtained with VMH instrument are presented for an interval of 3 days, starting with DOY 235. From upper to lower panels are depicted: the components of the interplanetary magnetic field in RTN coordinates (Br, Bt, Bn), and the absolute value of the magnetic field B, as well as their corresponding normalized variances (*i.e.*, $\sigma^2/|B|^2$).

Also, the magnetic field components present a well defined large-scale feature, that can be recognized in the behaviour of the relevant normalized variances. The presence of the ICME corresponds to a sudden drop in the magnetic field variances in the interval delimited by the two vertical solid lines in Fig.1 (panels 2, 4, 6, and 8).

In Fig.2 are plotted from top to bottom, the proton number density Np, the alpha to proton number density ratio (*i.e.*, $N(He++)/N(H+)$ ratio), solar wind bulk velocity Vp, the ratio of proton temperature Tp and the expected temperature $Texp$ (determined with the formula of Lopez (1987)), for an interval of 3 days starting with DOY 235. The data are obtained by SWOOPS instrument, with a 4 minute resolution.

In Figs. 1 and 2 the vertical dashed line corresponds to the shock arrival on 24 August 2001, at 8:00 UT (*i.e.* DOY 236.33). The boundaries of the magnetic cloud are indicated by the first vertical solid line, that corresponds to the start of the field coherent rotation (the beginning of the MC on 24 August 2001, at 13:00 UT), and the second vertical solid line, that corresponds to the ending for the rotation of magnetic

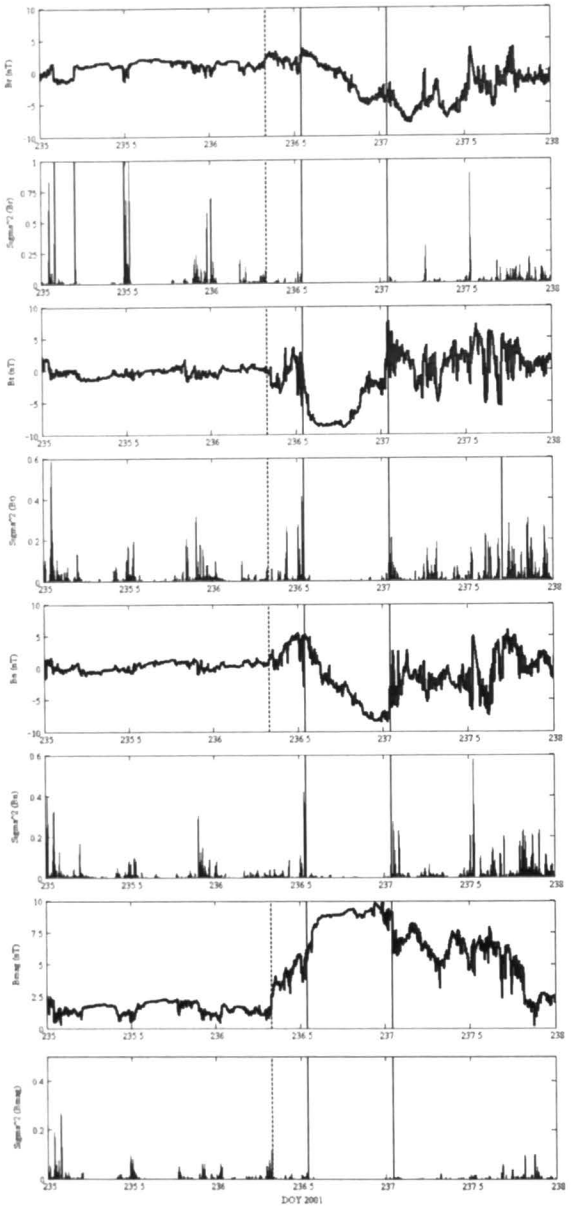

Fig. 1 – The magnetic field RTN components (Br, Bt, Bn), and magnetic field magnitude B, and the corresponding normalized variances for a time interval of 3 days.

field (end of the cloud on 25 August 2001, at 01:00 UT). In Fig. 2, the horizontal dashed line in the second panel, represents the 0.06 threshold (Hirshberg *et al.*, 1971;

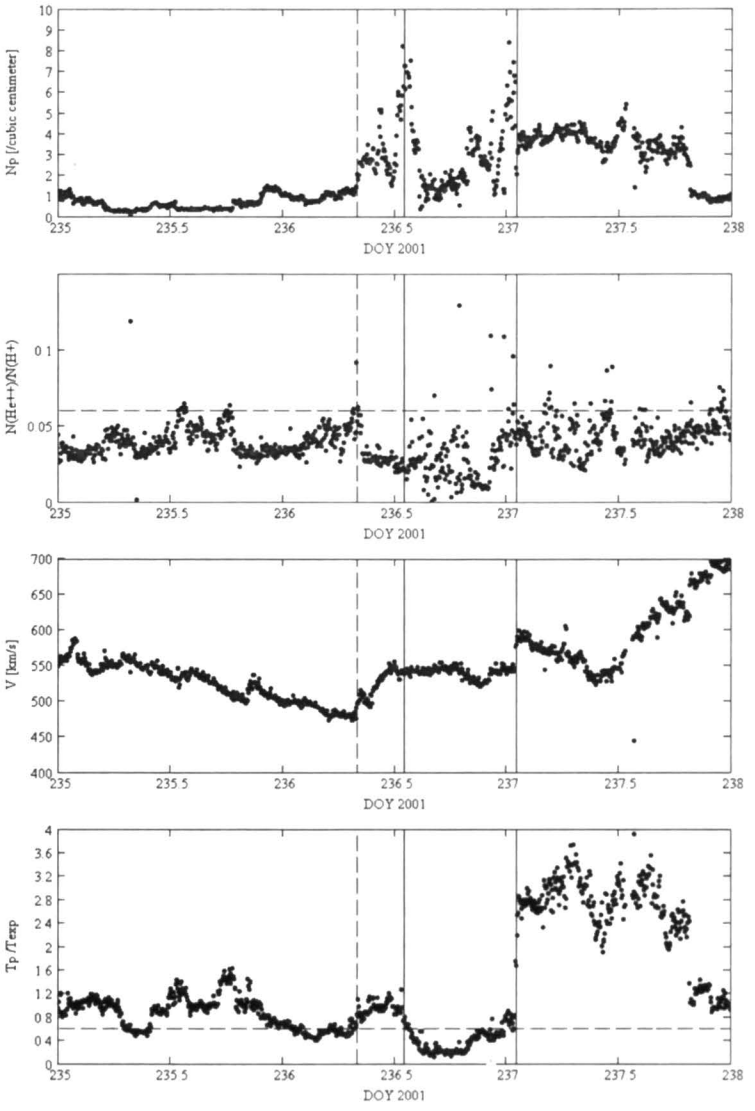

Fig. 2 – The proton number density Np, the alpha to proton number density ratio, solar wind bulk velocity Vp, and $Tp/Texp$, for a time interval of 3 days.

Borrini *et al.*, 1982) for the value of helium abundance.

Between the dashed line that corresponds to the shock arrival and the first solid vertical line, the sheath region is present. The arrival of a weak forward fast shock at Ulysses on DOY 236.33 can be observed in Fig. 1 and 2, this shock being identified in the data by the presence of discontinuities in the magnetic field intensity, proton

density, solar wind velocity, and proton temperature. These parameters present an increase at this time. During a time interval of 5 hours (between DOY 236.33 and DOY 236.542) the velocity is increasing from 475 km s^{-1} to 550 km s^{-1}. All these signatures indicate that immediately preceding the arrival of the MC, a hot, dense aggregation of the shocked sheath plasma is present.

The classical identification characteristics for an ICME can be observed in Figs. 1 and 2 during the interval between DOY 236.542 and DOY 237.042. The value of helium abundance (*i.e.* the alpha to proton number density ratio) is grater than 0.06 - 0.08. The criterion of abnormally low proton temperature (Tp) represents one of the primary ICME identification signatures. For the interval of the studied ICME, the proton temperature Tp follows the condition $Tp/Texp < 0.5$, where $Texp$ is calculated with the relations of Lopez (1987).

The condition stated by Richardson *et al.*(1997) regarding the proton (Tp) and electron (Te) temperatures (*i.e.*, $Te/Tp > 2$) is another indicator for the presence of an ICME. This condition is fulfilled by the studied event, according to Fig. 3 (top panel), that presents the comparison between the electron (steps) and proton (line) temperatures for a time interval of 3 days, starting with DOY 235.

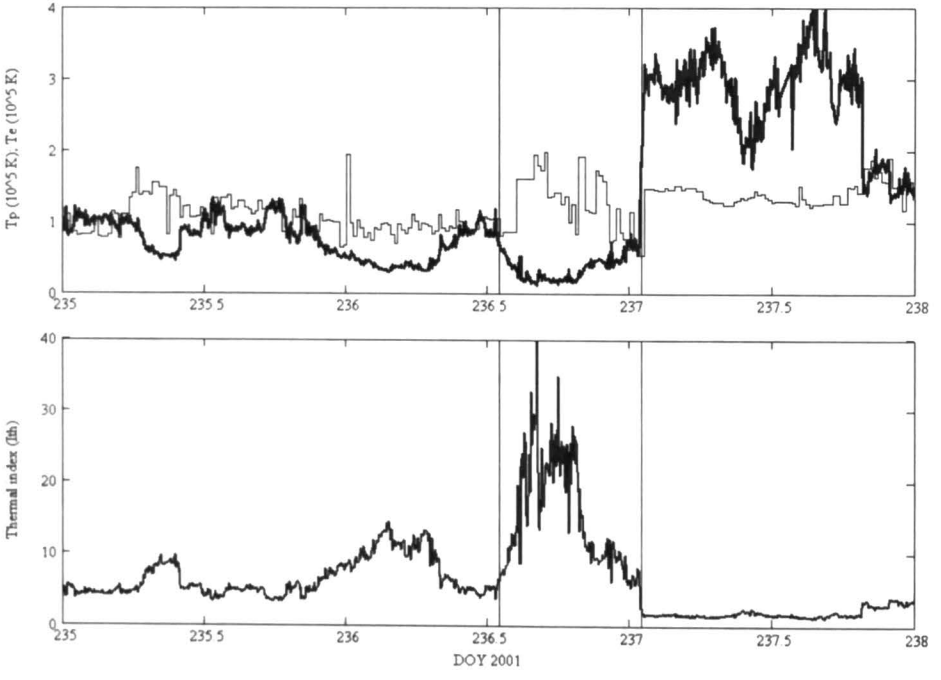

Fig. 3 – The comparison between the electron (steps) and proton (line) temperatures (top panel); the Ith thermal index (bottom panel), for a time interval of 3 days.

Plasma dynamics signature detection can be obtained using the *thermal index*, defined by Goldstein *et al.*(1998), as follows:

$$Ith = (500 \times Vp + 1.75 \times 10^5)/Tp \quad (1)$$

where Tp = plasma proton temperature; Vp = plasma proton velocity. If $Ith > 1$ plasma seems to be associated with an ICME (Goldstein *et al.*, 1998). Thermal index is a useful indicator because is mainly a result of the expansion of the plasma cloud as it propagates away from the sun.

In the case of the ICME registered on 24-25 August 2001, the thermal index riches very high values of about 35. The thermal index is displayed in Fig.3 (bottom panel), for a time interval of 3 days starting with DOY 235.

2.2. PLASMA COMPOSITION SIGNATURES ANALYSIS

For the plasma composition signatures detection, Popescu (2009) have used 3 hour averaged data for temperature, plasma composition and charge-state measurements of solar wind ions from SWICS instrument. This study is extended in this paper with new criteria of plasma composition signatures detection.

The present analysis underlines the following conclusions:

1) Criteria of low ion temperature is verified, in the studied interval of time all temperatures being low.

2) Heavy ion species present anomalies of abundance and charge state:

a) The optimum threshold value for the average Fe charge state is considered $< Q_{Fe} >= 11$ (Lepri and Zurbuchen, 2004). Greater values are indicators for the presence of ICMEs. The distributions of Fe average charge state and the Fe/O abundance are presented in Fig. 4 (top panel). In the studied interval of 5 days, the value of average iron charge state is between [10.5,11], and $Fe/O < 2$.

b) The enhanced charge-state ratios C(6+)/C(5+) and O(7+)/O(6+) can be observed in Fig. 4 (middle panel). Threshold O(7+)/O(6+) = 0.8 corresponds to a freezing-in temperature of 2.05×10^6 K, this condition being satisfied in the studied case. This result is in good agreement with the velocity distribution (in the studied interval of time the velocity is $\sim$ 550 km s^{-1}). In Fig.4 (middle panel) is also depicted with the continuous line the threshold established by Richardson and Cane (2004) for O(7+)/O(6+), in the case of an ICME:

$$O(7+)/O(6+) \geq 6.008 \times exp(-0.00578 \times Vp) \quad (2)$$

where Vp represents the solar wind bulk velocity.

For the 24 -25 August 2001 event, it is obvious that the charge-state ratios O(7+)/O(6+) is extremely high. Also, the charge-state ratios C(6+)/C(5+) is correlated with O(7+)/O(6+) ratio.

c) The enhancement of C(6+), Ne(8+), Mg(10+) densities relative to O(6+), can be observed in Fig.4 (bottom panel), for the quantities between the two vertical lines. Also, the criteria of Richardson and Cane (2004) have been also considered for Mg to O abundance ratio and Ne to O abundance ratio:

$$Mg/O > 0.982 \times exp(-0.00367 \times Vp) \quad (3)$$

$$Ne/O > 0.59 \times exp(-0.0017 \times Vp) \quad (4)$$

where Vp represents the solar wind bulk velocity.

Fig.4 (bottom panel) displays the Ulysses data for a 5 day interval, the upper dotted line representing the Ne/O abundance ratio obtained with the above formula, function of the solar wind speed. The lower continuous line represents the Mg to O abundance ratio determined with the formula of Richardson and Cane (2004). One observes that Mg/O is higher than this threshold, during the interval of the studied event. Only the condition for Mg/O is fulfilled in the case of the studied event.

The ICME registered on 24 - 25 August 2001 verifies almost all classical identification conditions, plasma dynamics and composition signatures. These signatures are not necessarily present simultaneously and define exact the same region of the solar wind. An enhanced helium abundance, depressed proton temperature, and smooth strong magnetic fields, compared with the ambient solar wind upstream of the shock, characterize this event.

3. STATISTICAL SCALING PROPERTIES OF INTERPLANETARY MAGNETIC FIELD TIME SERIES

In order to study the scaling and intermittency of the fluctuations for the magnetic field magnitude, B, and the RTN components (Br, Bt, Bn), we apply the finite size scaling technique on Ulysses data.

Intermittency refers to the statistical behaviour of the fluctuations in the spatial domain, but when the Taylor hypothesis is valid (*i.e.* a turbulent structure transits the space craft at a time which is small in comparison with its own evolution) time differences are equivalent to space differences.

In our study we consider the technique based on differencing of the original time series over a range of temporal scales τ. The fluctuations on temporal scale τ can be captured by a set of differences $dS(t,\tau) = S(t+\tau) - S(t)$, where $S(t)$ represents a given time series (Frisch, 1995).

First step in our calculation is represented by the determination of magnetic field magnitude differences, as well as for the RTN components Br, Bt, Bn, at a given scale $\tau_n = 2^n$ minutes ($n = 0, 1, 2, ..., 7$) through:

$$dB_n = dB_n(t_i, \tau_n) = [B(t_i + \tau_n) - B(t_i)] \quad (5)$$

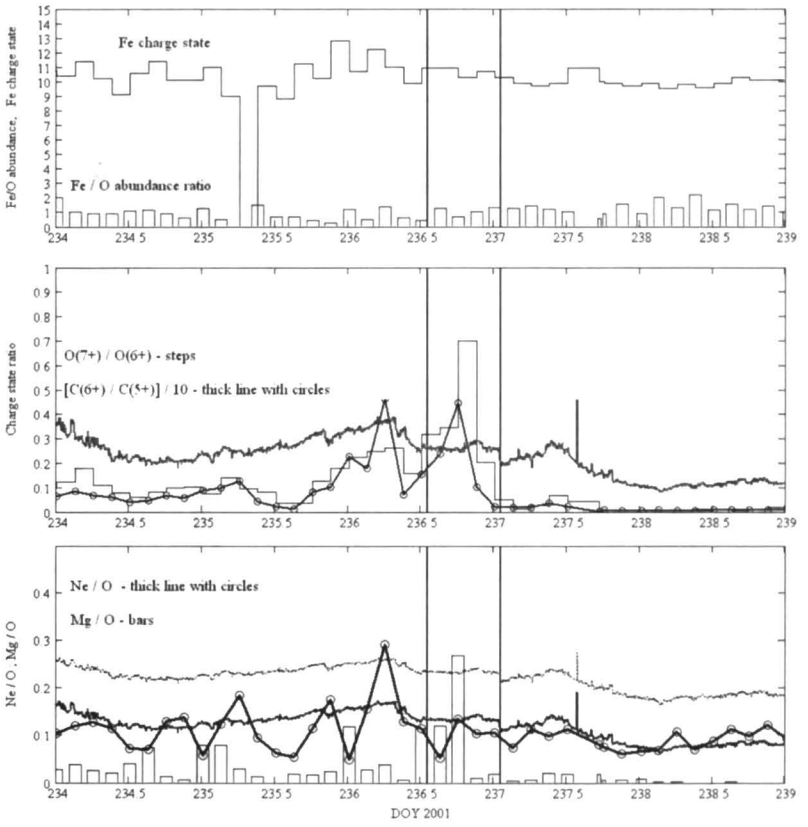

Fig. 4 – Fe average charge state and Fe/O abundance (top panel). Charge-state ratios C(6+)/C(5+) and O(7+)/O(6+) (middle panel). Ne(8+), Mg(10+) densities relative to O(6+)(bottom panel), for a time interval of 5 days, starting with DOY 234.

where t_i - the time (minutes); $B(t_i)$- the 1-minute resolution data for B, Br, Bt, Bn.

We considered scales ranging from $\tau_0 = 1$ minute to $\tau_7 = 2^7 = 128$ minutes ~ 2 hours, and obtained eight normalized data sets $dB_n(t_i, \tau_n)$, denoted $dB0$,...,$dB7$.

In Fig.5 the magnetic field magnitude differences $dB1$, $dB3$, $dB5$, $dB6$, $dB7$ for the magnetic field magnitude are plotted *versus* time (for a time interval of 3 days, starting with DOY 235).

3.1. PROBABILITY DISTRIBUTION FUNCTIONS

According to Marsch and Tu (1994), Sorriso-Valvo *et al.*(1999, 2001), both fast and slow solar wind streams are highly intermittent.

In the case of intermittent turbulent media, the probability distribution func-

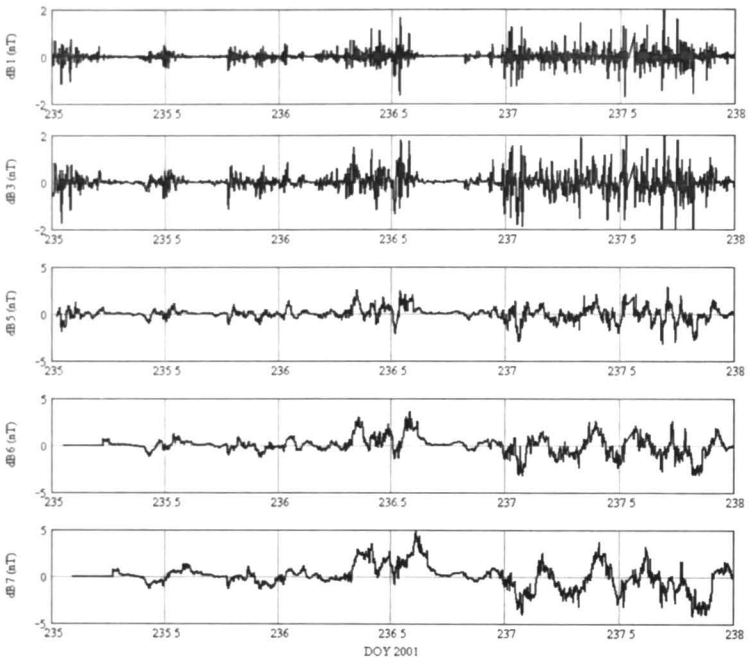

Fig. 5 – The magnetic field magnitude differences $dB1$, $dB3$, $dB5$, $dB6$, $dB7$ *versus* time, for a 3 days time interval.

tions (PDFs) of fluctuations have increasingly non-Gaussian shapes at smaller scales (Sorriso-Valvo *et al.*, 1999). Gaussian distributions for time lags longer than few hours fitt well the PDFs of the increments, while heavy-tailed shapes are present at scales smaller than few minutes. The fast streams are less intermittent than the slow wind flows, where the coherent structures are present and make the magnetic field fluctuations less random (Bruno *et al.*, 2003).

The properties of the intermittency of the magnetic turbulence in solar wind streams are strongly dependent on their regions of origin in the solar corona (Bruno *et al.*, 2003).

In Figs. 6, 7 and 8 are presented the unscaled PDFs of the magnetic field components dBr_n, dBt_n, dBn_n, respectively, for the considered time lags: $\tau_1 = 2$ minutes, $\tau_3 = 2^3 = 8$ minutes, $\tau_4 = 2^4 = 16$ minutes, $\tau_5 = 2^5 = 32$ minutes, $\tau_6 = 2^6 = 64$ minutes, and $\tau_7 = 2^7 = 128$ minutes. A time interval of 3 days, starting with DOY 235, is considered in our calculations. One observes at small scales the leptokurtic, long-tailed shapes of the PDFs. The values outside the core of the distribution especially rise from the major peaks of magnetic field fluctuations (see Popescu and Popescu, 2009).

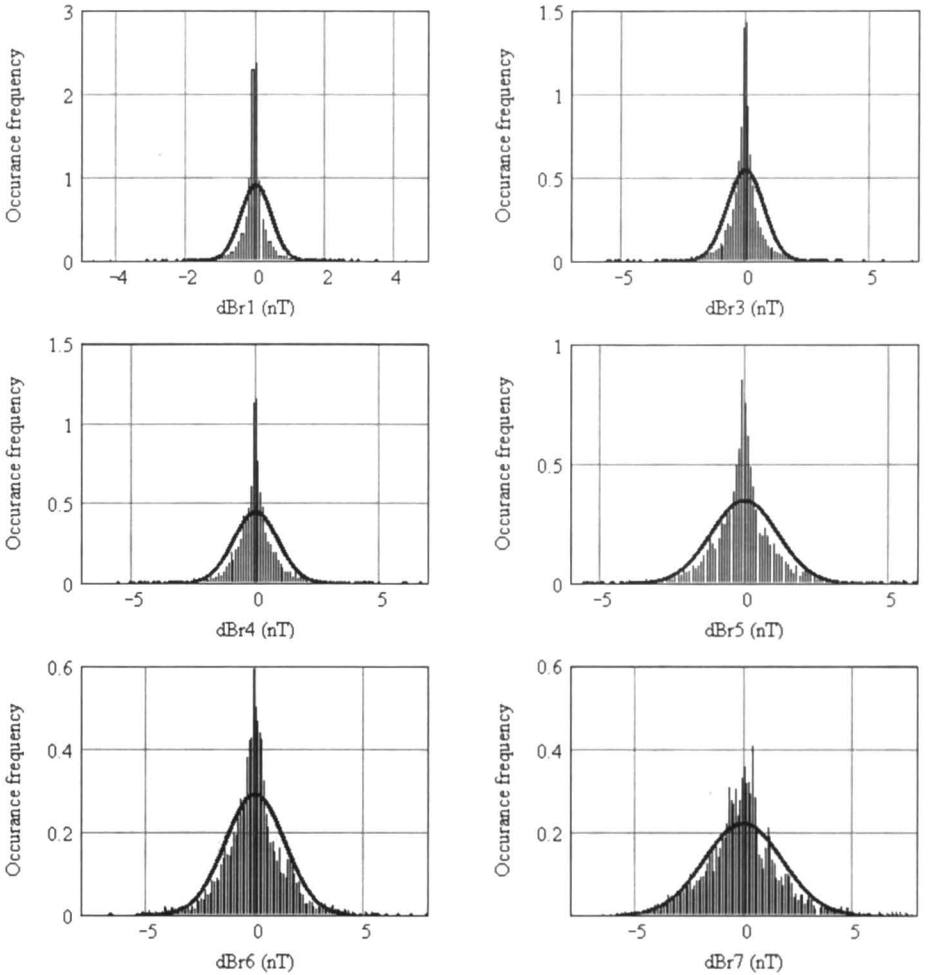

Fig. 6 – Unscaled PDFs for dBr_n, $n = 1, 3, 4, 5, 6, 7$ (bins of 0.1 nT are used for all lags).

3.2. GENERALIZED STRUCTURE FUNCTIONS ANALYSIS

We use high-order statistics to analyze the intermittent nature of the fluctuations. The generalized structure functions, particularly the third-order moment (skewness) and fourth-order moment (kurtosis), are important quantities to evaluate the degree of intermittency.

We have to mention that for Gaussian distribution the skewness and kurtosis equal zero, a positive (negative) skewness meaning a longer right (left) tail, and a positive (negative) kurtosis indicating a peaked (flat) distribution. A distribution with positive (negative) kurtosis is called leptokurtic (platykurtic).

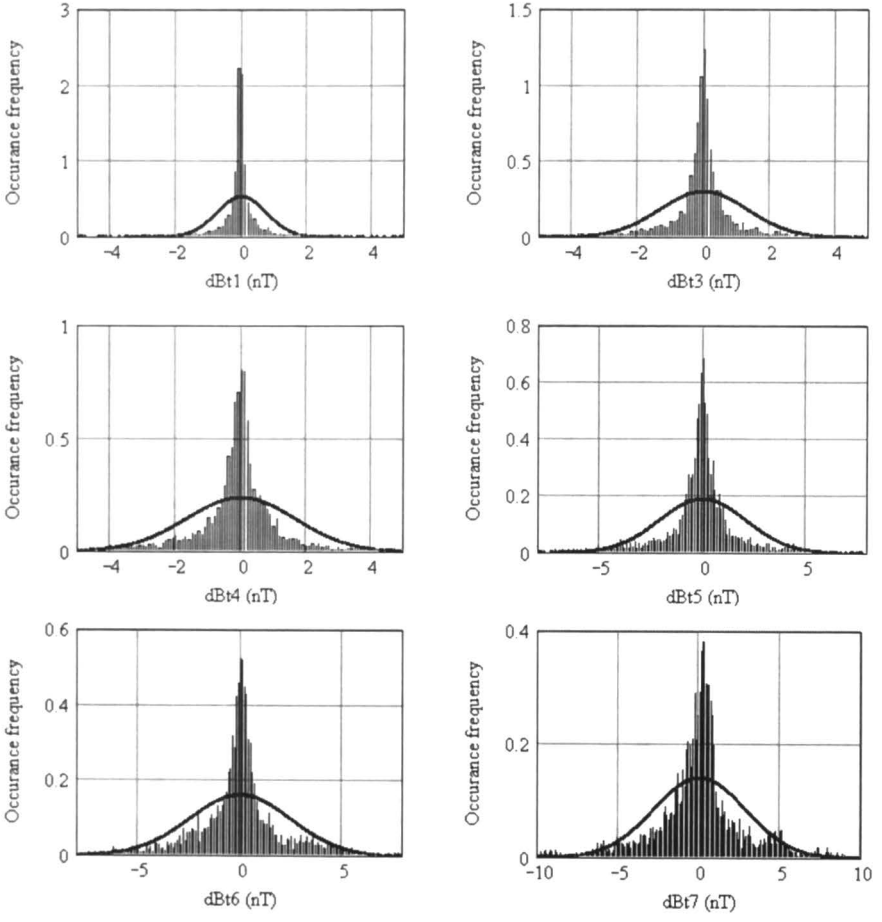

Fig. 7 – Unscaled PDFs for dBt_n, $n = 1, 3, 4, 5, 6, 7$ (bins of 0.1 nT are used for all lags).

The standard deviation, skewness, and kurtosis are plotted in Fig. 9 for the PDFs of the differences $dB_n(\tau_n)$, $dBr_n(\tau_n)$, $dBt_n(\tau_n)$, and $dBn_n(\tau_n)$, as a function of scale $n = log_2(\tau)$.

For the magnetic field magnitude and magnetic field components we can see a similar behaviour at all scales for the standard deviation and kurtosis (Fig.9 top and bottom panels).

As can be observed from Fig.9 (top panel) the standard deviation has an increasing trend with the increasing scale, with values between 1.2 nT and almost 3 nT, for $\tau_7 = 128$ minutes.

The kurtosis of $dB_n(\tau_n)$ and the other three magnetic field components differences is decreasing with increasing scale, at small scale a large kurtosis being

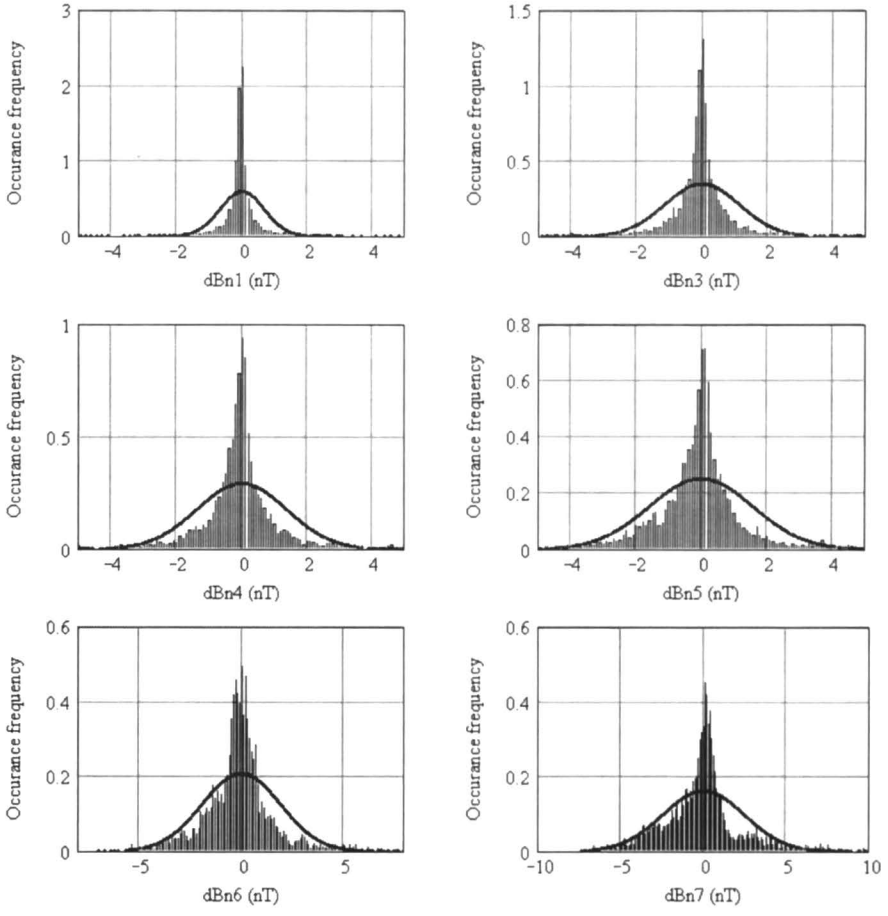

Fig. 8 – Unscaled PDFs for dBn_n, $n = 1, 3, 4, 5, 6, 7$ (bins of 0.1 nT are used for all lags).

associated with intermittent turbulence. The leptokurtic characteristics of PDFs for magnetic field fluctuations can be observed in Fig. 9 (bottom panel).

For $dBr_n(\tau_n)$, skewness presents negative values at small scales, its general values being in the interval [-2,0.5]. For $dB_n(\tau_n)$, $dBt_n(\tau_n)$, and $dBn_n(\tau_n)$, the skewness has mainly positive values, consistent with the shape of the distributions presented in Figs. 6, 7, and 8.

4. CONCLUSIONS

Multi-scale statistical methods such as PDFs analysis, and generalized structure functions have been considered for the study of interplanetary magnetic field

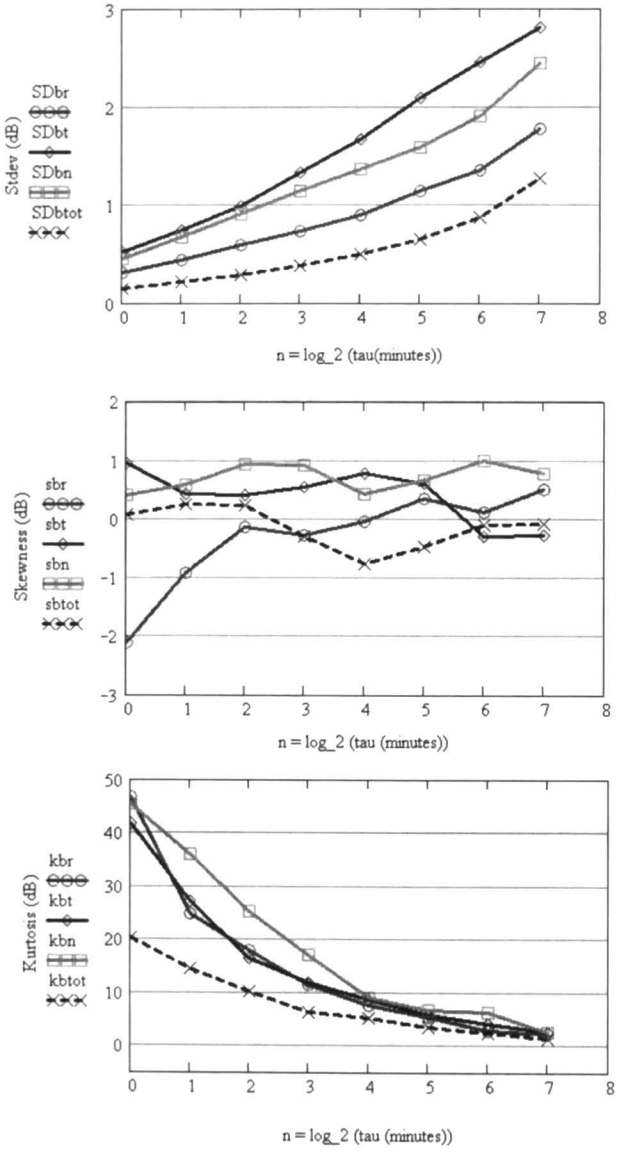

Fig. 9 – The high-order moments of dB_n, dBr_n, dBt_n, dBn_n as function of scale $n = log_2(\tau)$.

fluctuations, for the interval between DOY 235 - DOY 238, using data for the year 2001 from Ulysses/VHM instrument.

The fluctuations of the magnetic field magnitude (B), and the corresponding

RTN components (Br, Bt, Bn), at larger scales are less intermittent than at small scales. Their behaviour at different scales is quantitatively described by the probability distribution functions (PDFs) and generalized structure functions.

The values outside the core of the distribution especially rise from the major peaks of magnetic field fluctuations, caused mainly by the presence of the transient event on 24 - 25 August 2001 (DOY 236.542 - DOY 237.042). These values are mostly present at larger scales, $\tau_6 = 2^6 = 64$ minutes ~ 1 hour, and $\tau_7 = 2^7 = 128$ minutes ~ 2 hours, for Bt and Bn components of magnetic field. The analysis of the PDFs of the magnetic field increments revealed that the fourth-order moment of the distributions (*i.e.*, the kurtosis) increases as the time lag decreases.

The signatures of the ICME event that can be observed between DOY 236.542 - DOY 237.042 have been also analyzed. Almost all classical identification conditions, plasma dynamics and composition signatures have been verified by this ICME, that presents evident features of a magnetic cloud.

REFERENCES

Borrini, G., Gosling, J.T., Bame, S.J., and Feldman, W.C.: 1982, *J. Geophys. Res.* **87**, 7370.

Bruno, R., Carbone, V., Sorriso-Valvo, L., and Bavassano, B.: 2003, *J.Geophys. Res.* **108**, 1130.

Burlaga, L., Sittler, E., Mariani, F., and Schwenn, R.: 1981, *J. Geophys. Res.* **86**, 6673.

Burlaga, L.F.E.: 1991, *Physics of the Inner Heliosphere II*, 1.

Ebert, R.W., McComas, D.J., Elliott, H.A., Forsyth, R.J., and Gosling, J.T.: 2009, *J.Geophys. Res. A* **114**, 1109.

Feldman, U., Landi, E., and Schwadron, N.A.: 2005, *J.Geophys. Res.* **110**, 7109.

Frisch, U.: 1995, *Turbulence. The legacy of A. N. Kolmogorov., by Frisch, U.. Cambridge University Press, Cambridge (UK), 1995, XIII + 296 p., ISBN 0-521-45103-5.*

Goldstein, R., Neugebauer, M., and Clay, D.: 1998, *J. Geophys. Res.* **103**, 4761.

Hirshberg, J., Asbridge, J.R., and Robbins, D.E.: 1971, *Solar Phys.* **18**, 313.

Jones, G.H. and Balogh, A.: 2003, *Ann. Geophys.* **21**, 1377.

Lepri, S.T. and Zurbuchen, T.H.: 2004, *J.Geophys. Res. A* **109**, 6101.

Lopez, R.E.: 1987, *J. Geophys. Res.* **92**, 11189.

Marsch, E. and Tu, C.Y.: 1994, *Annales Geophysicae* **12**, 1127.

Neugebauer, M. and Snyder, C.W.: 1962, *Science* **138**, 1095.

Popescu, N.A. and Popescu, E.: 2009, *Romanian Astron. J.* **19**, 119.

Popescu, N.A.: 2009, *IAU Symposium* **257**, 295.

Richardson, I.G., Farrugia, C.J., and Cane, H.V.: 1997, *J. Geophys. Res.* **102**, 4691.

Richardson, I.G. and Cane, H.V.: 2004, *J.Geophys. Res.* **109**, 9104.

Sorriso-Valvo, L., Carbone, V., Veltri, P., Consolini, G., and Bruno, R.: 1999, *Geophys. Res. Lett.* **26**, 1801.

Sorriso-Valvo, L., Carbone, V., Giuliani, P., Veltri, P., Bruno, R., Antoni, V., and Martines, E.: 2001, *Planetary and Space Science* **49**, 1193.

Received on 5 October 2012

NEW REGULARIZATION OF THE RESTRICTED THREE-BODY PROBLEM

IHARKA SZÜCS-CSILLIK, RODICA ROMAN

Astronomical Institute of Romanian Academy
Astronomical Observatory of Cluj-Napoca
Str. Ciresilor 19,
RO-400487 Cluj-Napoca
Email: iharka@gmail.com; rdcroman@yahoo.com

Abstract. We find a very interesting transformation for regularization of the coordinates and time for the restricted three-body problem. The new regularization can give us significant informations regarding the behavior of the dynamical system near the singularity point.

Key words: Celestial Mechanics; Regularization.

1. INTRODUCTION

Regularization is originally defined as the elimination of singularities occurring in the equations of motion by properly selected variables (Szebehely, 1967). From Newton's law, we know that the bodies interact by means of a force which is proportional to the inverse of the squared distance. As the two bodies approach each other (close approach), their distance tends to zero and, consequently, the differential equation describing the dynamics of the system becomes singular when the two bodies collide. From the theoretical point of view, the singularity due to binary collisions between point masses can be handled by means of the regularization theory (Waldvogel, 1972; Érdi, 2004).

We know a lot of methods in the regularization theory for the 2-body problem, for instance the Euler method (Euler, 1765), Levi-Civita method (Levi-Civita, 1906) and the Kustaanheimo-Stiefel method (Kustaanheimo *et al.*, 1965). Many studies of the regularization problem are in the restricted 3-body problem, where we have 2 singularities. We can regularize local (one of them), or global. Birkhoff (1915); Thiele (1896); Burrau (1906); Lemaître (1955); Arenstorf (1963) and many other researchers studied the regularization of the restricted three-body problem (Aarseth *et al.*, 1974).

In this article we construct a new regularizing transformation, which depends on the right selection of the coordinates and time transformation. This new regularizing transformation has its own advantage compared to the Levi-Civita regularization, because it preserves the form of the regularized trajectory.

2. THE RESTRICTED THREE-BODY PROBLEM

Denoting S_1 and S_2 the components of the binary system (whose masses are m_1 and m_2), the equations of motion of the test particle (in the frame of the restricted three-body problem) in the coordinate system (S_1, x, y, z), (the physical plane) are (Roman *et al.*, 2012; Roman, 2011):

$$\frac{\mathrm{d}^2x}{\mathrm{d}t^2} - 2\frac{\mathrm{d}y}{\mathrm{d}t} = x - \frac{q}{1+q} - \frac{x}{(1+q)r_1^3} - \frac{q(x-1)}{(1+q)r_2^3} \tag{1}$$

$$\frac{\mathrm{d}^2y}{\mathrm{d}t^2} + 2\frac{\mathrm{d}x}{\mathrm{d}t} = y - \frac{y}{(1+q)r_1^3} - \frac{q\,y}{(1+q)r_2^3} \tag{2}$$

$$\frac{\mathrm{d}^2z}{\mathrm{d}t^2} = -\frac{z}{(1+q)r_1^3} - \frac{q\,z}{(1+q)r_2^3} \tag{3}$$

where

$$r_1 = \sqrt{x^2+y^2+z^2}\ ,\quad r_2 = \sqrt{(x-1)^2+y^2+z^2}\ ,\quad q = \frac{m_2}{m_1}. \tag{4}$$

These equations have singularities in the terms $\frac{1}{r_1}$ and $\frac{1}{r_2}$ (Mioc *et al.*, 2002; Csillik, 2003; Waldvogel, 1982, 2006). In order to regularize the equations (1)-(3), we introduce the generalized coordinates q_1, q_2, q_3 and generalized momenta p_1, p_2, p_3 (Boccaletti *et al.*, 1996; Roman *et al.*, 2012), and write the Hamiltonian and the canonical equations of motion:

$$\mathcal{H} = \frac{1}{2}(p_1^2+p_2^2+p_3^2) + p_1q_2 - q_1p_2 + \frac{q_1^2}{2} + \frac{q_2^2}{2} - \psi(q_1,q_2,q_3)\,. \tag{5}$$

Here

$$\Psi(q_1,q_2,q_3) = \frac{1}{2}\left[\left(q_1 - \frac{q}{1+q}\right)^2 + q_2^2 + \frac{2}{(1+q)r_1} + \frac{2q}{(1+q)r_2}\right], \tag{6}$$

with

$$r_1 = \sqrt{q_1^2+q_2^2+q_3^2},\quad r_2 = \sqrt{(q_1-1)^2+q_2^2+q_3^2}\,. \tag{7}$$

The generalized coordinates and the generalized momenta were:

$$q_1 = x\ ,\ q_2 = y\ ,\ q_3 = z\ ,\ p_1 = \dot{q_1} - q_2\ \ p_2 = \dot{q_2} + q_1\ ,\ p_3 = \dot{q_3}. \tag{8}$$

The canonical equations have the general form:

$$\dot{q_i} = \frac{\partial\mathcal{H}}{\partial p_i}\ ,\quad \dot{p_i} = -\frac{\partial\mathcal{H}}{\partial q_i}\ ,\quad i\in\{1,2,3\} \tag{9}$$

The canonical equations obtained from equations (1)-(3) have, in the (S_1, q_1, q_2, q_3) coordinate system, the explicit form:

$$\frac{\mathrm{d}q_1}{\mathrm{d}t} = p_1 + q_2 \tag{10}$$

$$\frac{\mathrm{d}q_2}{\mathrm{d}t} = p_2 - q_1 \tag{11}$$

$$\frac{\mathrm{d}q_3}{\mathrm{d}t} = p_3 \tag{12}$$

$$\frac{\mathrm{d}p_1}{\mathrm{d}t} = p_2 - \frac{q}{1+q} - \frac{1}{1+q}\cdot\frac{q_1}{r_1^3} - \frac{q}{1+q}\cdot\frac{q_1-1}{r_2^3} \tag{13}$$

$$\frac{\mathrm{d}p_2}{\mathrm{d}t} = -p_1 - \frac{1}{1+q}\cdot\frac{q_2}{r_1^3} - \frac{q}{1+q}\cdot\frac{q_2}{r_2^3} \tag{14}$$

$$\frac{\mathrm{d}p_3}{\mathrm{d}t} = -\frac{1}{1+q}\cdot\frac{q_3}{r_1^3} - \frac{q}{1+q}\cdot\frac{q_3}{r_2^3}. \tag{15}$$

For simplicity, we shall consider in what follows that the third body moves into the orbital plane ($z = 0$).

3. THE LEVI-CIVITA REGULARIZATION

We briefly present the well-known Levi-Civita regularization methods (Roman *et al.*, 2012). For the regularization of the equations of motion in the (q_1, S_1, q_2) coordinate system, we shall introduce new variables Q_1 and Q_2, connected with the coordinates q_1 and q_2 by the Levi-Civita equations (Levi-Civita, 1906):

$$q_1 = Q_1^2 - Q_2^2\,, \quad q_2 = 2Q_1Q_2\,, \tag{16}$$

Using Levi-Civita's coordinate transformation $f = q_1 = Q_1^2 - Q_2^2$, $g = q_2 = 2Q_1Q_2$, the equations of motion of the restricted three-body problem becomes:

$$\frac{\mathrm{d}Q_1}{\mathrm{d}t} = \frac{P_1}{D} + \frac{Q_2}{2} \tag{17}$$

$$\frac{\mathrm{d}Q_2}{\mathrm{d}t} = \frac{P_2}{D} - \frac{Q_1}{2} \tag{18}$$

$$\frac{\mathrm{d}P_1}{\mathrm{d}t} = \frac{P_2}{2} - \frac{2qQ_1}{1+q} - \frac{2}{1+q}\frac{Q_1}{\bar{r}_1^2} - \frac{2q}{1+q}\frac{Q_1(\bar{r}_1-1)}{\bar{r}_2^3} + \frac{(P_1^2+P_2^2)Q_1}{4\bar{r}_1^2} \tag{19}$$

$$\frac{\mathrm{d}P_2}{\mathrm{d}t} = -\frac{P_1}{2} + \frac{2qQ_2}{1+q} - \frac{2}{1+q}\frac{Q_2}{\bar{r}_1^2} - \frac{2q}{1+q}\frac{Q_2(\bar{r}_1+1)}{\bar{r}_2^3} + \frac{(P_1^2+P_2^2)Q_2}{4\bar{r}_1^2} \tag{20}$$

where

$$\begin{aligned} \bar{r}_1 &= Q_1^2 + Q_2^2 \\ \bar{r}_2 &= \sqrt{(Q_1^2 - Q_2^2 - 1)^2 + 4Q_1^2 Q_2^2} \end{aligned}$$

with the new Hamiltonian

$$\begin{aligned} \mathcal{H}_{S1} &= \frac{P_1^2 + P_2^2}{8(Q_1^2 + Q_2^2)} + \frac{1}{2}(P_1 Q_2 - P_2 Q_1) + \frac{q}{1+q}(Q_1^2 - Q_2^2) - \frac{1}{1+q} \cdot \\ &\cdot \frac{1}{Q_1^2 + Q_2^2} - \frac{q}{1+q} \cdot \frac{1}{\sqrt{(Q_1^2 - Q_2^2 - 1)^2 + 4Q_1^2 Q_2^2}} - \frac{q^2}{2(1+q)^2} \end{aligned} \quad (21)$$

Introducing a time transformation for the new equations of motion (17)-(20), the motion of the system is slowed down, in order to observe and study the movement of the system around the singularity points (Roman *et al.*, 2012; Mikkola *et al.*, 1996; Castilho *et al.*, 1999).

4. THE NEW REGULARIZATION

We propose a new regularizing transformation, to avoid the singularities from the equations of motion (10)–(11), (13)–(14). As in the Levi-Civita regularization method, we have two transformations for the regularization procedure: *coordinate transformation*, which gives the shape of the orbit, and *time transformation*, which makes the slow-down motion (Celletti *et al.*, 2011; Jiménez-Perez *et al.*, 2011).

4.1. COORDINATE TRANSFORMATION

The first step performed in the process of regularization consists in introduction of new coordinates Q_1 and Q_2. Let us introduce the generating function $\mathcal{S}$, (Stiefel *et al.*, 1971):

$$\mathcal{S} = -p_1 f(Q_1, Q_2) - p_2 g(Q_1, Q_2) \quad (22)$$

a $\mathcal{C}^2$ function. Here f and g are harmonic conjugated functions, with the property

$$\begin{aligned} \frac{\partial f}{\partial Q_1} &= \frac{\partial g}{\partial Q_2} \\ \frac{\partial f}{\partial Q_2} &= -\frac{\partial g}{\partial Q_1} \end{aligned}$$

The generating equations are

$$q_i = -\frac{\partial \mathcal{S}}{\partial p_i}, \quad P_i = -\frac{\partial \mathcal{S}}{\partial Q_i}, \quad i \in \{1,2\}, \quad (23)$$

with P_1, P_2 as new generalized momenta, or explicitly

$$\begin{aligned} q_1 &= \frac{\partial \mathcal{S}}{\partial p_1} = f(Q_1, Q_2) \\ q_2 &= \frac{\partial \mathcal{S}}{\partial p_2} = g(Q_1, Q_2) \\ P_1 &= \frac{\partial \mathcal{S}}{\partial Q_1} = p_1 \frac{\partial f}{\partial Q_1} + p_2 \frac{\partial g}{\partial Q_1} = p_1 a_{11} + p_2 a_{12} \\ P_2 &= \frac{\partial \mathcal{S}}{\partial Q_2} = p_1 \frac{\partial f}{\partial Q_2} + p_2 \frac{\partial g}{\partial Q_2} = -p_1 a_{12} + p_2 a_{11} \end{aligned} \tag{24}$$

where

$$\begin{aligned} a_{11} &= \frac{\partial f}{\partial Q_1} = \frac{\partial g}{\partial Q_2} \\ a_{12} &= -\frac{\partial f}{\partial Q_2} = \frac{\partial g}{\partial Q_1} \end{aligned}$$

Let us introduce the following notation:

$$A = \begin{pmatrix} a_{11} & a_{12} \\ a_{21} & a_{22} \end{pmatrix}, \quad D = detA = a_{11}^2 + a_{22}^2$$

The new Hamiltonian with the generalized coordinates Q_1 and Q_2 and the generalized momenta P_1 and P_2 is:

$$\begin{aligned} \mathcal{H}(Q_1, Q_2, P_1, P_2) &= \frac{1}{2D}\left[P_1^2 + P_2^2 + P_1 \frac{\partial}{\partial Q_2}(f^2+g^2) - P_2 \frac{\partial}{\partial Q_1}(f^2+g^2)\right] + \\ &+ \frac{q}{1+q} f - \frac{1}{1+q} \cdot \frac{1}{\overline{r}_1} - \frac{q}{1+q} \cdot \frac{1}{\overline{r}_2} - \frac{q^2}{2(1+q)^2} \end{aligned} \tag{25}$$

where

$$\overline{r}_1 = \sqrt{f^2+g^2}\,, \quad \overline{r}_2 = \sqrt{(f-1)^2+g^2}\,, \quad D = \left(\frac{\partial f}{\partial Q_1}\right)^2 + \left(\frac{\partial g}{\partial Q_1}\right)^2.$$

In our new method of regularization, the new variables Q_1 and Q_2, are connected with the coordinates q_1 and q_2 by the *hyperbolical transformation*:

$$q_1 = \sin(Q_1)\cosh(Q_2)\,, \quad q_2 = \cos(Q_1)\sinh(Q_2). \tag{26}$$

The equations (26) transform the points $S_1(0;0)$ and $S_2(1;0)$ from the physical plane, into the points $S_1(0;0)$ and $S_2(1.57;0)$ in the regularized plane.

Then, the canonical equations (10)–(11), (13)–(14) become:

$$\frac{dQ_1}{dt} = \frac{P_1}{D} + \frac{\sinh(2Q_2)}{2D} \tag{27}$$

$$\frac{dQ_2}{dt} = \frac{P_2}{D} - \frac{\sin(2Q_1)}{2D} \tag{28}$$

$$\begin{aligned}\frac{dP_1}{dt} &= -\frac{P_1^2+P_2^2}{2}\cdot\frac{\sin(2Q_1)}{D^2} - \frac{P_1}{2}\cdot\frac{\sinh(2Q_2)\sin(2Q_1)}{D^2} + \\ &+ \frac{P_2}{D}\cdot\cos(2Q_1) + \frac{P_2}{2}\cdot\frac{\sin^2(2Q_1)}{D^2} - \\ &- \frac{q}{1+q}\cdot\cos(Q_1)\cosh(Q_2) - \frac{1}{2(1+q)}\cdot\frac{\sin(2Q_1)}{\overline{r}_1^3} + \\ &+ \frac{q}{1+q}\cdot\frac{\cos(Q_1)\cdot(\sin(Q_1)-\cosh(Q_2))}{\overline{r}_2^3}\end{aligned} \tag{29}$$

$$\begin{aligned}\frac{dP_2}{dt} &= \frac{P_1^2+P_2^2}{2}\cdot\frac{\sinh(2Q_2)}{D^2} + \frac{P_1}{2}\cdot\frac{\sinh^2(2Q_2)}{D^2} - \frac{P_1}{D}\cdot\cosh(2Q_2) - \\ &- \frac{P_2}{2}\cdot\frac{\sin(2Q_1)\sinh(2Q_2)}{D^2} - \frac{q}{1+q}\cdot\sin(Q_1)\sinh(Q_2) - \\ &- \frac{1}{2(1+q)}\cdot\frac{\sinh(2Q_2)}{\overline{r}_1^3} + \frac{q}{1+q}\cdot\frac{\sinh(Q_2)\cdot(\sin(Q_1)-\cosh(Q_2))}{\overline{r}_2^3}\end{aligned} \tag{30}$$

where

$\overline{r}_1 = \sqrt{\frac{\cosh(2Q_2)-\cos(2Q_1)}{2}}$, $\overline{r}_2 = |\cosh(Q_2)-\sin(Q_1)|$, $D = \cos^2(Q_1)+\sinh^2(Q_2)$
with the new Hamiltonian:

$$\begin{aligned}\mathcal{H}_{S1} &= \frac{1}{2D}\left[P_1^2+P_2^2+P_1\sinh(2Q_2)-P_2\sin(2Q_1)\right] + \\ &+ \frac{q}{1+q}\sin(Q_1)\cosh(Q_2) - \frac{1}{1+q}\cdot\frac{1}{\overline{r}_1} - \frac{q}{1+q}\cdot\frac{1}{\overline{r}_2} - \frac{q^2}{2(1+q)^2}\end{aligned} \tag{31}$$

For the hyperbolic regularization we can postulate the following theorem:

Theorem

The hyperbolic regularization preserves the form of the trajectory of the test particle, if the initial coordinates Q_{10} and Q_{20} have absolute values smaller than 1.

Proof:

Expanding into Taylor's series the equations (26) writen for the initial position, we obtain:

$$q_{10} = Q_{10} + \frac{Q_{10}\cdot Q_{20}^2}{2} - \frac{Q_{10}^3}{6} + \frac{Q_{10}\cdot Q_{20}^4}{24} - \frac{Q_{10}^3\cdot Q_{20}^2}{12} + \frac{Q_{10}^5}{120} + \frac{Q_{10}\cdot Q_{20}^6}{720} - \frac{Q_{10}^7}{5040}\ldots$$

$$q_{20} = Q_{20} + \frac{Q_{20}\cdot Q_{10}^2}{2} - \frac{Q_{20}^3}{6} + \frac{Q_{20}\cdot Q_{10}^4}{24} - \frac{Q_{20}^3\cdot Q_{10}^2}{12} + \frac{Q_{20}^5}{120} + \frac{Q_{20}\cdot Q_{10}^6}{720} - \frac{Q_{20}^7}{5040}\ldots$$

If $Q_{10} < 1$ and $Q_{20} < 1$ we obtain $q_{10} \approx Q_{10}$ and $q_{20} \approx Q_{20}$. So, the initial positions into the physical plane and into the hyperbolical regularized plane have similar coordinates. Idem for initial momenta. So, the trajectories are resemblant.

4.2. TIME TRANSFORMATION

The second step performed in the process of regularization consists in the time transformation. In order to solve the Hamiltonian equations (27)-(30), we introduce the fictitious time τ, and making the time transformation $\frac{dt}{d\tau} = \overline{r}_1^3\overline{r}_2^2$, the new regular equations of motion become:

$$\begin{aligned}
\frac{dQ_1}{d\tau} &= \left(\frac{P_1}{D} + \frac{\sinh(2Q_2)}{2D}\right)\overline{r}_1^3\overline{r}_2^2 \\
\frac{dQ_2}{d\tau} &= \left(\frac{P_2}{D} - \frac{\sin(2Q_1)}{2D}\right)\overline{r}_1^3\overline{r}_2^2 \\
\frac{dP_1}{dt} &= \left(-\frac{P_1^2+P_2^2}{2}\cdot\frac{\sin(2Q_1)}{D^2} - \frac{P_1}{2}\cdot\frac{\sinh(2Q_2)\sin(2Q_1)}{D^2} + \frac{P_2}{D}\cdot\cos(2Q_1) + \right. \\
&+ \frac{P_2}{2}\cdot\frac{\sin^2(2Q_1)}{D^2} - \frac{q}{1+q}\cdot\cos(Q_1)\cosh(Q_2) - \frac{1}{2(1+q)}\cdot\frac{\sin(2Q_1)}{\overline{r}_1^3} + \\
&+ \left.\frac{q}{1+q}\cdot\frac{\cos(Q_1)\cdot(\sin(Q_1)-\cosh(Q_2))}{\overline{r}_2^3}\right)\overline{r}_1^3\overline{r}_2^2 \\
\frac{dP_2}{dt} &= \left(\frac{P_1^2+P_2^2}{2}\cdot\frac{\sinh(2Q_2)}{D^2} + \frac{P_1}{2}\cdot\frac{\sinh^2(2Q_2)}{D^2} - \frac{P_1}{D}\cdot\cosh(2Q_2) - \right. \\
&- \frac{P_2}{2}\cdot\frac{\sin(2Q_1)\sinh(2Q_2)}{D^2} - \frac{q}{1+q}\cdot\sin(Q_1)\sinh(Q_2) - \frac{1}{2(1+q)}\cdot \\
&\left.\frac{\sinh(2Q_2)}{\overline{r}_1^3} + \frac{q}{1+q}\cdot\frac{\sinh(Q_2)\cdot(\sin(Q_1)-\cosh(Q_2))}{\overline{r}_2^3}\right)\overline{r}_1^3\overline{r}_2^2
\end{aligned} \tag{32}$$

Now, the equations of motion of the test particle do not have singularities.

5. APPLICATION

In order to emphasize the advantage of the hyperbolical regularization, we made a numerical application, for the Earth-Moon binary system, which is characterized by the mass ratio $q = 0.0123$. We integrated the equations of motion (10)–(11) and (13)–(14) in the physical plane (S_1, q_1, q_2), considering the initial conditions:

$$q_{10} = -0.5\,, \quad q_{20} = 0.1\,, \quad p_{10} = -0.5\,, \quad p_{20} = -0.5\,.$$

The trajectory of a mass point is given in Figure 1, where P_0 represents the initial position. The initial conditions for equations (27)-(30) are obtained by solving the

systems:

$$\begin{cases} q_{10} &= \sin(Q_{10})\cdot\cosh(Q_{20}) \\ q_{20} &= \cos(Q_{10})\cdot\sinh(Q_{20}) \end{cases},$$

$$\begin{cases} P_{10} &= p_{10}\cos(Q_{10})\cosh(Q_{20}) - p_{20}\sin(Q_{10})\sinh(Q_{20}) \\ P_{20} &= p_{10}\sin(Q_{10})\sinh(Q_{20}) + p_{20}\cos(Q_{10})\cosh(Q_{20}) \end{cases}$$

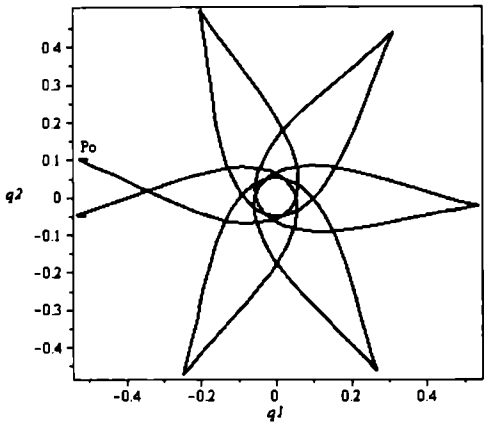

Fig. 1 – The trajectory of the test particle in the physical plane. Here, $P_0(-0.5;0.1)$.

By consequence, the equations of motion (27)-(30) must be integrated with initial conditions:

$$Q_{10} = -0.52\,,\quad Q_{20} = 0.11\,,\quad P_{10} = -0.46\,,\quad P_{20} = -0.41\,.$$

The trajectory of a mass point in the regularized plane (S_1, Q_1, Q_2) is given in Fig.2a. This trajectory can be compared with the one obtained by applying the Levi-Civita's method, integrating the equations (17)-(20), and is given in Fig.2b.

The initial conditions for equations (17)–(20), (Levi-Civita case) are obtained by solving the systems:

$$\begin{cases} q_{10} &= Q_{10}^2 - Q_{20}^2 \\ q_{20} &= 2Q_{10}Q_{20} \end{cases}, \quad \begin{cases} P_{10} &= 2p_{10}Q_{10} + 2p_{20}Q_{20} \\ P_{20} &= -2p_{10}Q_{20} + 2p_{20}Q_{10} \end{cases}$$

The corresponding initial conditions in the Levi-Civita case are:

$$Q_{10} = -0.07\,,\quad Q_{20} = -0.71\,,\quad P_{10} = 0.78\,,\quad P_{20} = -0.64\,.$$

It is easy to remark that the hyperbolic regularization preserves the form of the trajectory better than the Levi-Civita method (Fig.1 and 2a are very similar).

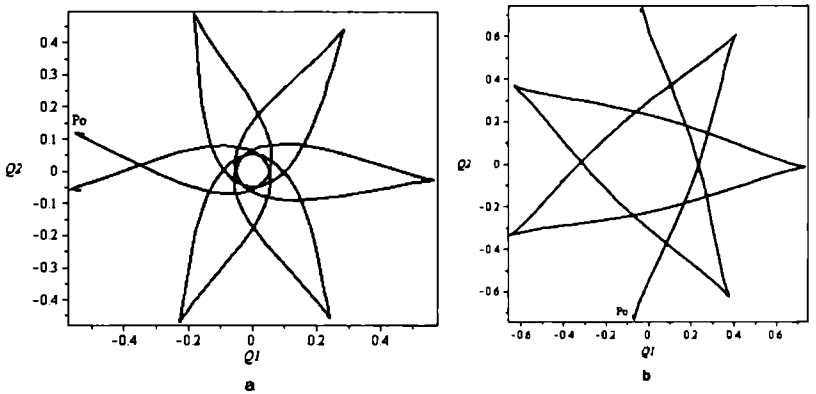

Fig. 2 – The trajectory of the test particle in the regularized plane, using (a) the hyperbolic regularization (where $P_0(-0.52;0.11)$) and (b) the Levi-Civita regularization (where $P_0(-0.07;-0.71)$).

6. CONCLUSION

Comparing the hyperbolic regularizing transformation and the Levi-Civita regularization, we remark that the shape of the orbit is different. When we want to apply a regularization method, we choose the best method for our problem, the method which gives us more information about the motion near the singularity points. In a critical singularity point, the study in a regularized plane is recommended, because many numerical integrators avoid the singularity point. Our proposed new regularization method, called *the hyperbolical regularization* is a very simple and fast method, which preserves very well the shape of the orbits, and can be effectively used in the phase space to examine a close approach (collision).

REFERENCES

Aarseth, S.J., and Zare, K.: 1974, *Celest. Mech. Dyn. Astron.* **10**, 185
Arenstorf, R.F.: 1963, *Astron. J.* **68**, 548
Birkhoff, G.D.: 1915, *Rend. Circ. Mat. Palermo* **39**, 1
Boccaletti, D., and Pucacco, G.: 1996, *Theory of orbits* **1**. Springer-Verlag Berlin Heidelberg New York
Burrau, C.: 1906, *Vierteljahrschrift Astron. Ges.* **41**, 261
Castilho, C., and Vidal, C.: 1999, *Qual. Theory Dyn. Syst.* **1**, 1
Celletti, A., Stefanelli, L., Lega, E., and Froeschlé, C.: 2011, *Celest. Mech. Dyn. Astron.* **109**, 265
Csillik, I.: 2003, *Regularization methods in celestial mechanics*. House of the Book of Science Cluj
Euler, L.: 1765, *Nov. Comm. Petrop.* **11**, 144
Érdi, B.: 2004, *Celest. Mech. Dyn. Astron.* **90**, 35
Jiménez-Perez, H., and Lacomba, E.: 2011, *J. Phys. A* **44**, 265
Kopal, Z.: 1978, *Dynamics of Close Binary Systems*. Reidel, Dordrecht

Kustaanheimo, P., and Stiefel, E. L.: 1965, *J. Reine Angewandte Math.* **218**, 204
Lemaître, G.: 1955, *Vistas in Astronomy* **1**, 207
Levi-Civita, T.: 1906, *Acta Mathematica* **30**, 305
Mikkola, S., Aarseth, S.J.: 1996, *Celest. Mech. Dyn. Astron.* **64**, 197
Mioc, V., and Csillik, I.: 2002, *Romanian Astron. J.* **12**, 167
Roman, R.: 2011, *Astrophys. Space Sci.* **335**, 475
Roman, R., and Szücs-Csillik, I.: 2012, *Astrophys. Space Sci.* **338**, 233
Stiefel, L., and Scheifele, G.: 1971 *Linear and regular celestial mechanics*. Springer Berlin
Szebehely, V.: 1967, *Theory of orbits*. Academic Press, New York
Szebehely, V.: 1975, *Lecture Notes in Mathematics* **461**, 257
Thiele, T.N.: 1896, *Astron. Nachr.* **138**, 1
Waldvogel, J.: 1982, *Celest. Mech. Dyn. Astron.* **28**, 69
Waldvogel, J.: 1972, *Celest. Mech. Dyn. Astron.* **6**, 221
Waldvogel, J.: 2006, *Celest. Mech. Dyn. Astron.* **95**, 201

Received on 31 October 2012

AN EQUATION FOR ASTRONOMICAL DETERMINATION OF THE MOMENTS OF INERTIA OF THE EARTH

IERONIM MIHĂILĂ

University of Bucharest, Faculty of Mathematics and Computer Science
Str. Academiei 14,
010014 Bucharest, Romania
Email: mihaila@fmi.unibuc.ro

Abstract. Using the properties of invariance of the moments of inertia with respect to the reduction of the equation of the ellipsoid of inertia to the canonical form, an equation for determination of the polar moment of inertia is established. Thus the number of equations for determination of the moments of inertia from the five harmonic coefficients of the second degree of the geopotential is equal to the number of unknowns. On the other hand, it is shown that the assumption of Erzhanov and Kalybaev concerning a certain relation between the moments of inertia about the axes of the geocentric coordinate system in which the series of the potential is given and the dynamical flattening is justified. New formulae for determination of the Eulerian angles concerning the orientation of the ellipsoid of inertia are obtained. The moments of inertia in the case of the Standard Earth II are computed.

Key words: geopotential - moments of inertia of the Earth - dynamical flattening.

1. INTRODUCTION

Theoretically, if the density distribution inside the Earth is a known function, its moments of inertia can be computed. The difficulty consists in the fact that this function is unknown, and it is necessary to make different assumptions about the Earth's internal constitution. A first approximation is obtained considering the Earth homogeneous. Improved values of the moments can be obtained considering the Earth constituted of homogeneous layers and the density a piecewise continuous and decreasing function from the center to the surface.

A possibility for a more precise determination of the moments of inertia of the Earth is offered by the series of the geopotential obtained by means of the Earth's artificial satellites. The five harmonic coefficients of the second degree, which are determined from observations, depend of the six unknown moments of inertia. Therefore, using these harmonic coefficients, one obtains five equations for the six moments of inertia. The system of equations would be complete if a new equation is added. Erzhanov and Kalybaev (1975, 1984) proposed the equation $[C' - (A' + B')/2]/C' = H$, where the dynamical flattening H is obtained from the constant of lunisolar precession and A', B', C' are the unknown moments of inertia with re-

spect to the geocentric coordinate system in which the series is given. But, because $H = [C-(A+B)/2]/C$, A, B, C being the principal moments of inertia, it is necessary to prove that $[C'-(A'+B')/2]/C'$ can be replaced by H. In the present paper, this assumption is proved. For this purpose, using the properties of invariance of the moments with respect to the reduction of the equation of the ellipsoid of inertia to the canonical form, an equation for determination of the polar moment is established. Then new formulae concerning the orientation of the ellipsoid of inertia are obtained, and the moments of inertia for the Standard Earth II are computed.

2. THE GEOPOTENTIAL AND THE MOMENTS OF INERTIA

In the geocentric coordinate system $O\xi\eta\zeta$, in which the axis $O\zeta$ is oriented toward the Conventional International Origin, and the plane $O\xi\zeta$ is the origin plane for longitude (Greenwich meridian plane), the gravitational potential of the Earth is given by the series

$$\begin{aligned} U(r,\varphi,\lambda) &= \frac{GM}{r}\Big[1-\sum_{n=2}^{\infty}\Big(\frac{a_e}{r}\Big)^n J_n P_n(\sin\varphi) \\ &\quad +\sum_{n=2}^{\infty}\sum_{k=1}^{n}\Big(\frac{a_e}{r}\Big)^n P_n^{(k)}(\sin\varphi)(C_{nk}\cos k\lambda + S_{nk}\sin k\lambda)\Big], \end{aligned} \tag{1}$$

where G is the gravitational constant, M and a_e are the mass and the equatorial radius of the Earth, P_n is the polynomial of Legendre of n^{th} degree, and $P_n^{(k)}$ is the associated function of Legendre of n^{th} degree and k^{th} order. On the other hand, r, λ, φ are the polar coordinates, r being the geocentric distance, λ the longitude and φ the geocentric latitude.

The harmonic coefficients of the second degree can be expressed in function of the moments of inertia. One obtains the following relations

$$\begin{aligned} Ma_e^2 J_2 &= C' - \frac{A'+B'}{2}, \\ 4Ma_e^2 C_{22} &= B'-A', \\ Ma_e^2 C_{21} &= E', \\ Ma_e^2 S_{21} &= D', \\ 2Ma_e^2 S_{22} &= F'. \end{aligned} \tag{2}$$

These five relations and the relation proposed by Erzhanov and Kalybaev,

$$H = \frac{C'-(A'+B')/2}{C'}, \tag{3}$$

allow the determination of the moments A', B', C', D', E', F'. For the moments of

inertia in the system $O\xi\eta\zeta$ we keep the notations utilized by Erzhanov and Kalybaev (1984), namely

$$\begin{aligned} A' &= \int_V \rho(\xi,\eta,\zeta)(\eta^2+\zeta^2)\mathrm{d}v, \\ B' &= \int_V \rho(\xi,\eta,\zeta)(\xi^2+\zeta^2)\mathrm{d}v, \\ C' &= \int_V \rho(\xi,\eta,\zeta)(\xi^2+\eta^2)\mathrm{d}v, \\ D' &= \int_V \rho(\xi,\eta,\zeta)\zeta\eta\mathrm{d}v, \\ E' &= \int_V \rho(\xi,\eta,\zeta)\zeta\xi\mathrm{d}v, \\ F' &= \int_V \rho(\xi,\eta,\zeta)\xi\eta\mathrm{d}v, \end{aligned} \tag{4}$$

where V is the domain occupied by the Earth and ρ is the density.

The presented form of the geopotential has been recommended by the International Astronomical Union (Hagihara, 1962). But in the papers consecrated to the determination of the coefficients of the geopotential is frequently used the following form (Aksenov, 1977)

$$\begin{aligned} U = \frac{GM}{r}[1 &- \sum_{n=2}^{\infty}\left(\frac{a_e}{r}\right)^n J_n P_n(\sin\varphi) \\ &+ \sum_{n=2}^{\infty}\sum_{k=1}^{n}\left(\frac{a_e}{r}\right)^n p_n^{(k)}(\sin\varphi)(\overline{C}_{nk}\cos k\lambda + \overline{S}_{nk}\sin k\lambda)], \end{aligned} \tag{5}$$

where $p_n^{(k)}$ is the fully normalized associated function of Legendre, and the coefficients $\overline{C}_{nk}$ and $\overline{S}_{nk}$ have the expressions

$$\begin{aligned} \overline{C}_{nk} &= \sqrt{\frac{(n+k)!}{2(n-k)!}}\frac{C_{nk}}{\sqrt{2n+1}}, \\ \overline{S}_{nk} &= \sqrt{\frac{(n+k)!}{2(n-k)!}}\frac{S_{nk}}{\sqrt{2n+1}}. \end{aligned} \tag{6}$$

We mention that the geopotential can be also represented by another series (Erzhanov and Kalybaev, 1984; Mueller, 1964).

For the normalized coefficients of the second degree one obtains

$$\begin{aligned} \overline{C}_{21} &= \sqrt{\frac{3}{5}}C_{21},\ \overline{S}_{21} = \sqrt{\frac{3}{5}}S_{21}, \\ \overline{C}_{22} &= \sqrt{\frac{12}{5}}C_{22},\ \overline{S}_{22} = \sqrt{\frac{12}{5}}S_{22}. \end{aligned} \tag{7}$$

3. AN EQUATION FOR DETERMINATION OF THE POLAR MOMENT OF INERTIA

The five relations (2) are insufficient to determine the six moments of inertia. For this reason it is necessary to deduce another equation.

In the geocentric coordinate system $O\xi\eta\zeta$, the equation of ellipsoid of inertia is

$$A'\xi^2 + B'\eta^2 + C'\zeta^2 - 2D'\eta\zeta - 2E'\xi\zeta - 2F'\xi\eta = 1. \tag{8}$$

In the system $Oxyz$, defined by the principal axes of inertia, the equation becomes

$$Ax^2 + By^2 + Cz^2 = 1, \tag{9}$$

A, B, C being the principal moments of inertia, which can be determined by solving the secular equation

$$\begin{vmatrix} A'-q & -F' & -E' \\ -F' & B'-q & -D' \\ -E' & -D' & C'-q \end{vmatrix} = 0 \tag{10}$$

or

$$\begin{aligned} &q^3 - (A'+B'+C')q^2 + \\ &+(A'B' + A'C' + B'C' - D'^2 - E'^2 - F'^2)q - \\ &-(A'B'C' - 2D'E'F' - A'D'^2 - B'E'^2 - C'F'^2) = 0. \end{aligned} \tag{11}$$

Because the values A, B, C of the principal moments of inertia do not depend on the orientation of the system $O\xi\eta\zeta$, it results that the coefficients of the secular equation are invariant. Therefore we can write

$$\begin{aligned} A+B+C &= A'+B'+C', \\ AB+AC+BC &= A'B' + A'C' + B'C' - D'^2 - E'^2 - F'^2, \\ ABC &= A'B'C' - 2D'E'F' - A'D'^2 - B'E'^2 - C'F'^2. \end{aligned} \tag{12}$$

From the expression of the dynamical flattening

$$H = \frac{C - (A+B)/2}{C} \tag{13}$$

one obtains

$$C = \frac{A+B}{2(1-H)}. \tag{14}$$

On the other hand, taking into account the relations

$$\begin{aligned} A+B+C &= A'+B'+C', \\ Ma_e^2 J_2 &= C' - (A'+B')/2, \end{aligned}$$

we obtain

$$C = \frac{3C' - 2J_2 Ma_e^2}{3-2H}. \tag{15}$$

From the relations $AB+AC+BC = AB+(A+B)C = h$, $ABC = k$, where h and k are the values of the corresponding invariants, we can write $AB = k/C$ and $k/C + (A+B)C = h$, and therefore $A+B = h/C - k/C^2$. Substituting this expression of A+B in the expression (14) of C, it results

$$2(1-H)C^3 - hC + k = 0 \tag{16}$$

or

$$\begin{aligned} 2(1 - H)&\left(\frac{3C' - 2J_2 Ma_e^2}{3-2H}\right)^3 \\ &- \frac{3C' - 2J_2 Ma_e^2}{3-2H}(A'B' + A'C' + B'C' - D'^2 - E'^2 - F'^2) \\ &+ A'B'C' - 2D'E'F' - A'D'^2 - B'E'^2 - C'F'^2 = 0. \end{aligned} \tag{17}$$

But, from the relations $A'+B' = 2C' - 2J_2 Ma_e^2 = 2C' + a'$, $B' - A' = 4Ma_e^2 C_{22} = b'$, where $a' = -2J_2 Ma_e^2$ and $b' = 4Ma_e^2 C_{22}$ are known, one obtains

$$\begin{aligned} A' &= C' + \frac{a'-b'}{2}, \\ B' &= C' + \frac{a'+b'}{2}. \end{aligned} \tag{18}$$

Substituting in the last equation, this becomes

$$ax^3 + bx^2 + cx + d = 0, \tag{19}$$

where

$$
\begin{aligned}
x &= C', \\
a &= 8H^3, \\
b &= 8H^3 a', \\
c &= -2H(3-4H)a'^2 + 2H(3-2H)^2\left(\frac{a'^2-b'^2}{4} - D'^2 - E'^2 - F'^2\right), \\
d &= -2(1-H)a'^3 + (3-2H)^2 a'\left(\frac{a'^2-b'^2}{4} - D'^2 - E'^2 - F'^2\right) + \\
&\quad + (3-2H)^3\left(2D'E'F' + \frac{a'+b'}{2}E'^2 + \frac{a'-b'}{2}D'^2\right).
\end{aligned} \tag{20}
$$

Because for the models of geopotential $a > 0$, $b < 0$, $c < 0$, $d < 0$, according to Descartes' rule of signs, the obtained equation (19) has only one positive root.

The system of six independent equations (2) and (19) allows the determination of the moments of inertia A', B', C', D', E', F'. On the other hand, solving the secular equation one obtains the principal moments A, B, C.

Because the Earth's mass is determined with a less accuracy, it is preferably to use the normalized moments of inertia $\overline{A}' = A'/Ma_e^2$, etc., and the normalized values $\overline{a}' = a'/Ma_e^2 = -2J_2$, $\overline{b}' = b'/Ma_e^2 = 4C_{22}$. In this case, the equation (19) becomes

$$\bar{a}\bar{x}^3 + \bar{b}\bar{x}^2 + \bar{c}\bar{x} + \bar{d} = 0, \tag{21}$$

where

$$
\begin{aligned}
\overline{x} &= \overline{C}', \\
\overline{a} &= 8H^3, \\
\overline{b} &= 8H^3\overline{a}', \\
\overline{c} &= -2H(3-4H)\overline{a}'^2 + 2H(3-2H)^2\left(\frac{\overline{a}'^2-\overline{b}'^2}{4} - \overline{D}'^2 - \overline{E}'^2 - \overline{F}'^2\right), \\
\overline{d} &= -2(1-H)\overline{a}'^3 + (3-2H)^2\overline{a}'\left(\frac{\overline{a}'^2-\overline{b}'^2}{4} - \overline{D}'^2 - \overline{E}'^2 - \overline{F}'^2\right) + \\
&\quad + (3-2H)^3\left(2\overline{D}'\overline{E}'\overline{F}' + \frac{\overline{a}'+\overline{b}'}{2}\overline{E}'^2 + \frac{\overline{a}'-\overline{b}'}{2}\overline{D}'^2\right).
\end{aligned} \tag{22}
$$

Evidently, $\overline{H} = [\overline{C} - (\overline{A}+\overline{B})/2]/\overline{C} = H$. The equations (2) become

$$
\begin{aligned}
\overline{C}' - \frac{(\overline{A}'+\overline{B}')}{2} &= J_2, \\
\overline{B}' - \overline{A}' &= 4C_{22}, \\
\overline{D}' &= S_{21}, \\
\overline{E}' &= C_{21}, \\
\overline{F}' &= 2S_{22}.
\end{aligned} \tag{23}
$$

On the other hand, in the case of the normalized moments the secular equation has the same form and give the normalized principal moments $\overline{A}$, $\overline{B}$, $\overline{C}$.

We mention that the value of C' obtained by means of the deduced equation (Vîlcu, 2009) practically coincides with the value obtained taking into account the relation $[C' - (A' + B')/2]/C' = H$. Thus the relation proposed by Erzhanov and Kalybaev is justified. Evidently, because the moments D', E', F' are very small in comparison with the moments A', B', C', practically $[C' - (A' + B')/2]/C' = [C - (A + B)/2]/C = H$. But in the general case it is necessary to use the obtained equation for the polar moment.

4. ORIENTATION OF THE ELLIPSOID OF INERTIA

The orientation of the ellipsoid of inertia, *i.e.* the orientation of the principal axes of inertia with respect to the system $O\xi\eta\zeta$ can be given either by spherical coordinates (longitude and geocentric latitude) or by the Eulerian angles. We shall use the second possibility, as in the work of Erzhanov and Kalybaev (1984), but in a different manner. Let $\beta = (\widehat{O\xi, ON})$, $\alpha = (\widehat{ON, Ox})$, $\gamma = (\widehat{O\zeta, Oz})$ be the Eulerian angles, ON being the line of intersection between the planes $O\xi\eta$ and Oxy.

Let $(\gamma_{i1}, \gamma_{i2}, \gamma_{i3})$ $(i = 1,2,3)$ be the direction cosines of the principal axes of inertia Ox, Oy, Oz with respect to $O\xi\eta\zeta$. They have the following expressions

$$\begin{aligned}
\gamma_{11} &= \cos\beta\cos\alpha - \sin\beta\sin\alpha\cos\gamma, \\
\gamma_{12} &= \sin\beta\cos\alpha + \cos\beta\sin\alpha\cos\gamma, \\
\gamma_{13} &= \sin\alpha\sin\gamma, \\
\gamma_{21} &= -\cos\beta\sin\alpha - \sin\beta\cos\alpha\cos\gamma, \\
\gamma_{22} &= -\sin\beta\sin\alpha + \cos\beta\cos\alpha\cos\gamma, \\
\gamma_{23} &= \cos\alpha\sin\gamma, \\
\gamma_{31} &= \sin\beta\sin\gamma, \\
\gamma_{32} &= -\cos\beta\sin\gamma, \\
\gamma_{33} &= \cos\gamma,
\end{aligned} \tag{24}$$

and are given by the relations

$$\frac{\gamma_{i1}}{\delta_{i1}} = \frac{\gamma_{i2}}{\delta_{i2}} = \frac{\gamma_{i3}}{\delta_{i3}} = \frac{1}{(\delta_{i1}^2 + \delta_{i2}^2 + \delta_{i3}^2)^{1/2}}, \tag{25}$$

where $\delta_{i1}, \delta_{i2}, \delta_{i3}$ (i=1,2,3) are the cofactors of the elements in the row i of the determinant Δ which appears in the secular equation, q being successively replaced by A, B, C. On the other hand, the system $Oxyz$ has the same orientation as the system

$O\xi\eta\zeta$, if the following condition is fulfilled (Efimov, 1972)

$$\begin{vmatrix} \gamma_{11} & \gamma_{12} & \gamma_{13} \\ \gamma_{21} & \gamma_{22} & \gamma_{23} \\ \gamma_{31} & \gamma_{32} & \gamma_{33} \end{vmatrix} = 1. \tag{26}$$

Once determined the direction cosines, one can obtain the Eulerian angles by the formulae

$$\begin{aligned} \cos\gamma &= \gamma_{33}, \\ \sin\alpha\sin\gamma &= \gamma_{13}, \\ \cos\alpha\cos\gamma &= \gamma_{23}, \\ \sin\beta\sin\gamma &= \gamma_{12}\gamma_{23} - \gamma_{22}\gamma_{13}, \\ \cos\beta\sin\gamma &= \gamma_{11}\gamma_{23} - \gamma_{21}\gamma_{13}. \end{aligned} \tag{27}$$

We mention that analogous formulae are used for determination of the angular elements in the methods of orbit determination.

If $\gamma = 0$, then the plane Oxy coincides with $O\xi\eta$, and the orientation of the ellipsoid is reduced to the orientation of the ellipse of inertia. From (24) it is results

$$\begin{aligned} \gamma_{11} &= \cos(\beta+\alpha) = \cos\lambda, \\ \gamma_{12} &= \sin(\beta+\alpha) = \sin\lambda, \\ \gamma_{21} &= -\sin(\beta+\alpha) = -\sin\lambda, \\ \gamma_{22} &= \cos(\beta+\alpha) = \cos\lambda, \end{aligned} \tag{28}$$

where λ is the longitude of the axis Ox in the plane $O\xi\eta$.

Evidently, if the direction cosines are determined, then the orientation of the principal axes can be also given by spherical coordinates, as in the case of velocity ellipsoid of the stars (Mihaila, 1974).

5. STANDARD EARTH II

For to give an example, we present the results obtained for the geopotential model concerning the Standard Earth II (Gaposhkin and Lambeck, 1970), a model analyzed by Erzhanov and Kalybaev. For this model the geocentric gravitational constant $GM = 3.986013 \times 10^{-14}\mathrm{m}^3\mathrm{s}^{-2}$ and the equatorial radius $a_e = 6378155$ m. On the other hand, the harmonic coefficients of the second degree have the values $J_2 = 1082.628 \times 10^{-6}$, $\overline{C}_{21} = \overline{S}_{21} = 0$, $\overline{C}_{22} = 2.41290 \times 10^{-6}$, $\overline{S}_{22} = -1.36410 \times 10^{-6}$.

We shall use the value of the dynamical flattening given by Petit and Luzum (2010), namely $H = 0.003273795$. One obtains for the normalized moments of in-

ertia

$$\begin{aligned} \overline{A}' &= 0.329609368, \\ \overline{B}' &= 0.329615598, \\ \overline{C}' &= 0.330695111, \\ \overline{D}' &= \overline{E}' = 0, \\ \overline{F}' &= -1.761045528 \times 10^{-6}. \end{aligned} \tag{29}$$

Solving the secular equation, it results for the normalized principal moments

$$\begin{aligned} \overline{A} &= 0.329608907, \\ \overline{B} &= 0.329616059, \\ \overline{C} &= 0.330695111. \end{aligned} \tag{30}$$

Using the value of the gravitational constant $G = 6.67428 \times 10^{-11} m^3 \mathrm{kg}^{-1} \mathrm{s}^{-2}$, adopted in the IAU(2009) System of astronomical constants, we obtain for the principal moments of inertia (in $10^{37} \mathrm{kg} \cdot \mathrm{m}^2$)

$$\begin{aligned} A &= 8.007187118, \\ B &= 8.008160879, \\ C &= 8.034376902. \end{aligned} \tag{31}$$

The values of the moments are given with nine or ten significant digits only to obtain H with seven significant digits. We note anew that the value of the polar moment C' obtained by means of the deduced equation practically coincides with the value given by the Erzhanov and Kalybaev relation, the difference being at most of the order of 10^{-9} for the normalized moment.

In the case of the Standard Earth II, because the angle $\gamma = 0$, the orientation of the ellipsoid of inertia is reduced to the orientation of the ellipse of inertia in the equatorial plane. One obtains for the longitude of the axis corresponding to the minimum moment (A) the value $\lambda = -14.7^0$. The obtained results are slightly different from the results obtained by Erzhanov and Kalybaev (1984), who used the value $H = 0.00327364$ for the dynamical flattening.

We mention that the equation was already used for different models of geopotential (Vîlcu, 2009).

6. CONCLUSION

In the present paper an equation for determination of the polar moment of inertia of the Earth is obtained. The equation contains the dynamical flattening, which are deduced from the constant of lunisolar precession. According to Descartes' rule

of signs, this cubic equation has only one positive root. The value of the normalized polar moment deduced by solving the equation practically coincides with the value obtained taking into account the relation proposed by Erzhanov and Kalybaev, the difference being at most of the order of 10^{-9}. Therefore their assumption is justified.

The cause consists in the fact that the product of inertia (D', E', F') are very small in comparison with the moments about the axes (A', B', C'). We mention that the obtained equation is exact not only in this case, but also in the general case. On the other hand, the given formulae regarding the orientation of the ellipsoid of inertia allow the univocal determination of the Eulerian angles.

REFERENCES

Aksenov, E. P.: 1977, *Theory of the motion of Earth's artificial satellites*, Nauka, Moscow [in Russian].

Efimov, N. V.: 1972, *Quadratic forms and matrices*, Nauka, Moscow [in Russian].

Erzhanov, Zh. S., Kalybaev, A. A.: 1975, *Doklady Akademii Nauk SSSR*, **223**, 844.

Erzhanov, Zh. S., Kalybaev, A. A.: 1984, *General theory of the rotation of the Earth*, Nauka, Moscow [in Russian].

Gaposhkin, E. M., and Lambeck, K.: 1970, *Smithsonian Inst. Astrophys. Obs.*, Special Report No. **315**.

Hagihara, Y.: 1962, *Astron. J.*, **67**, 108.

Mihaila, I.: 1974, *Celest. Mech.*, **10**, 345.

Mueller, I.: 1964, *Introduction to satellite geodesy*, Frederick Ungar Publ. Co., New York.

Petit, G., Luzum, B. (eds.): 2010, *IERS Conventions (2010)*, Verlag des Bundesamts für Kartographie und Geodäsie, Frankfurt am Main.

Vîlcu, A. D.: 2009, *An. Univ. Bucuresti Mat.*, **58**, 183.

Received on 4 February 2013

THE SUN WORSHIP WITH THE ROMANIANS

DOINA IONESCU, CRISTIANA DUMITRACHE

Astronomical Institute of Romanian Academy
Str. Cutitul de Argint 5,
40557 Bucharest, Romania
Email: doinaionescu36@yahoo.com,
crisd@aira.astro.ro

Abstract. We summarize the main aspects of the solar cult with the Romanian people and the populations that lived on their territory. We highlight the origin of the solar cult and its evidence with the ancestors of the Romanians, the Dacians, as well as its manifestations in present popular art and other aspects of Romanians life.

Key words: astronomy history, Sun.

1. INTRODUCTION

The Sun, our day star, has always impressed people all over the world, who included it in their cultures. The Sun gives warmth, light, life and therefore it is associated with a powerful symbolism in all forms of culture. There are many studies concerning the worshipping of the Sun in different cultures such as the ancient Egyptian, Aztec, Asian, Greek, as well as in the European countries. We note here the book of Bhatnagar and Livingston (2005), that presents a nice review of solar worship all over the world.

One can speak about the existence of a solar cult on the territory of Romania beginning with ancient times, more precisely with the Neolithic. This cult was taken over by the Romanians ancestors, called the Getae-Dacians, and it has continued to exist until nowadays.

First, let us say a word about the ancient inhabitants of Romania. The hearth of present day Romania was initially inhabited by the Getae, a branch of the Thracians, a people of Indo-European origin who were archaeologically attested on the territory between the Balkan Mountains (South), The Forest Mountains (North), the Black Sea shore (East) and beyond the river Siret (West). They were firstly mentioned by the Greek historian Herodotus, who presented them as being situated on the territories South of the Danube in 514 BC, when the Persian king Darius launched a campaign against the Scythes, which inhabited the shore of the Black Sea. Strabon, in his work *Geographica*, made a more exact presentation of the Getaes frontiers. He called some of the Getae by the name of Dacians, the more widely spread name of the Romanians ancestors. Their country was located in the area in and around the

Carpathian Mountains and East of there to the Black Sea.

Densuşianu (1913) noted that a powerful Neolithic migration, coming from Central Asia, had formed its first European country at the Carpathians, "at the Lower Danube and especially in the countries of Dacia". This was the Pelasgian population that formed and coalesced the great and powerful centre of the Neolithic population in Europe.

It seems that in our country the solar cult was first attested with the Pelasgians, forefathers of the Getae-Dacians, that lived in the Eastern part of the Get-Dacian territory, mainly around the Island of Leuce (the present Island of the Snakes, in the Black Sea). Homer placed Boreas in Thrace, and, therefore, in his opinion, the land of Hyperborea was somewhere to the North of the Thracian territory, perhaps in Dacia. The historic Hecateus Abderita, who lived in the time of Alexander the Great (4th-3rd century BC), showed that the population from the islands of the North Sea had raised a great circular temple to a native Apollo, a god of light and fire. He said that the priests of Apollo were the sons of Boreas (Georgescu, 2011). The Hyperboreans worship of Apollo is considered to be the golden epoch of the ante-Greek Pelasgian civilization.

In 1823, the archaeologists discovered on the Leunce island plateau the ruins of a square temple, with the sides of almost 30 meters, made up of big stone blocks, joined without cement, just as the Dacians built their fortresses. This temple was surrounded by many annexes intended for the storage of the gifts the people brought to their God of Sun.

In the territory inhabited by the Getae, a country later called Dacia, the solar cult appeared as part of an ample process of Indo-Europeanization, brought about first by the Scythes, by the end of the 3rd century BC. They had an Uranian religion that worshipped the Sun. Later it was enforced by the Celtic tribes, who conquered and settled for a while on part of the Get-Dacians territory in the 2nd century BC. The Celts had a real cult of the Sun, attested also during their presence in Gallia and Ireland that lasted until the appearance of Christianity. They worshipped a solar god was called Belenus, a god of light and fire . All these Scythe and Celtic influences added to the already formed Get-Dacian background, where the worshipping of the Sun already manifested.

2. THE GETAE- DACIANS

On the territory of our country, archaeological researches revealed in isolated Getae, Scythe and Celtic tombs, as well as in great such necropolis, the existence of a great number of solar symbols on amulets, pottery, arms or many other kinds of objects. The multitude of these solar proofs is explained by the fact that the solar

cult, actually of a distant Indo-European origin, was a strong characteristic of the Get-Dacians religion.

All the symbols of the solar cult (the disk, sun wheel, swastika, spiral, boat, chariot, swan, and ax) were found in considerable number almost everywhere on the territory of Dacia. This solar cult reached its peak at the epoch of the metals, especially starting from the Epoch Age. We present below (Fig.1) two ancient Dacian objects bearing clear solar symbols. One is a Dacian silver coin, over 2200 years old, where a solar wheel with a solar horse is represented, that was found at Voloscani, Vidra village, Vrancea county, and in Moldavia (Silvia Păun, 1999). Another symbol is a Sun wheel with eight radii imprinted on a Dacian iron nail head, over 2100 years old, found at Sarmizegetusa Regia, Hunedoara country, Transylvania.

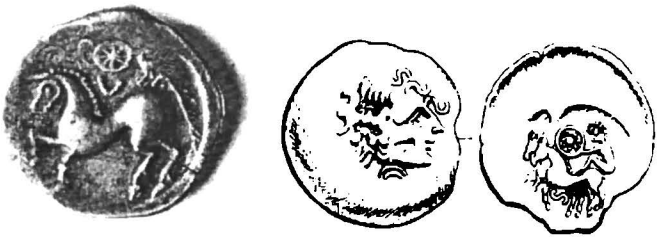

Fig. 1 – Dacian coin with sun wheel and solar horse, representing Apollo, the god of Sun.

The Sun wheel is common to many people, but the swastika symbol, a kind of solar wheel, seems to be an old Arian symbol. Citing Wikipedia encyclopedia we note that "The genesis of the swastika symbol is often treated in conjunction with cross symbols in general, such as the sun cross of pagan Bronze Age religion". There are a few speculative hypotheses and one of them is that the cross symbols and the swastika share a common origin in simply symbolizing the Sun (http://en.wikipedia.org/wiki/Swastika#Origin_hypotheses). This symbol comes from the places between the Danube and the Carpathians Mountains,the so-called Dacia Hyperborea, at around 3000 BC. The Sun stronghold from Leuce Island (The *Alba* Monastery) is represented on a coin that has an ox head and the swastika sign on one of the sides. The swastika represents an ancient solar symbol, but, analyzing now this old sign, we cannot help observing that the interplanetary magnetic field has the same design at the maximum of the solar activity. Consequently, we can say that the swastika represents the Sun and the solar influence over the planetary space. This symbolism has been preserved, being still marked on popular bred in some religious rituals (Fig.2).

A special solar symbol, manifest beginning with the end of the Bronze Age is the so-called aquatic bird (swan or duck), that usually draws a solar chariot. The

Fig. 2 – Swastika, the symbol of the Sun and its influence, an ancient hyperborean sign.

solar chariots appeared in the Near Orient and spread over a vast area. With the Getae-Dacians the solar cult symbolized by the swan carrying a boat or a solar chariot perpetuated until the first Iron Age, and it can be found in many parts of Dacia. Worth mentioning are two very interesting discoveries, namely two miniature solar chariots made of bronze, with iron spindles, drawn by eight aquatic birds. The first such chariot was discovered near the town of Oraştie (Transylvania), in 1834. The second similar object was found in a funeral tomb at the village of Bujoru, the county of Teleorman, South of Romania, in 1974 (Fig.3).

The solar chariot found at Bujoru is made of bronze and it has iron spindles. It is made up of a frame with four wheels, on which is placed an elongated vase with lid, where incinerations were made for the solar god. The chariot was adorned at the ends with aquatic birds. The heads of such birds adorned also the nails that fixed the chariot. It was dated back to the Bronze Age and is considered to be a complex image of the solar god Apollo the Hyperborean. At the epoch of Herodotus there was the tradition of Apollo, the Hyperborean God, who, in winter, left on his chariot drawn by swans to the frozen North, to come back in spring.

Solar symbols are also present on the pottery discovered at Grădiştea Muncelului, within the remnants of the old Dacians' capital, Sarmizegetusa. All these manifestations of the solar cult from the Bronze Age certainly evolved, but there rises the question whether they can be connected to the Great God of the Getae-Dacians, Zalmoxis. We know from historical sources that Zalmoxis was considered a god of the sky and of light. Consequently he must have been also the god of the Sun, of fire and life, both here on earth, as well as in eternal life. He was also the patron of astronomy and a former student of Pythagoras. He and the great priest Deceneus, the latter one from the epoch of King Burebista (1st century BC), were the ones that taught astronomy to the Getae-Dacians.

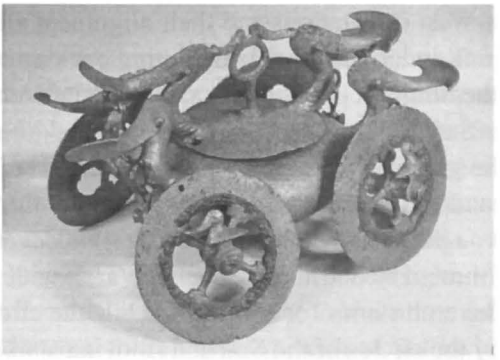

Fig. 3 – Solar chariot discovered at Bujoreni (Bronze Age).

Part of this astronomical knowledge became manifest also in the construction of sanctuaries. Sarmizegetusa Regia, the capital of the Dacian state, is made up of a complex of sanctuaries and a civil settlement, dating from the Neolithic Age. The sanctuaries were dedicated to the cult of the Sun and to astronomical observations. The constructions there made up an ingenious calendar, surprisingly precise for the respective epoch.

The complex of sanctuaries, seven in number is situated at an altitude of 1200 m, in the Orăştie Mountains, on an artificially terraced plateau. All this was kept away from the uninitiated's eyes, and seems to have been intended for the deciphering of the astral mechanisms and of the great cosmic cycles. These sanctuaries correspond to the five naked-eye visible planets: Mercury, Venus, Mars, Jupiter, Saturn; there is also one that corresponds to the Moon, whereas the seventh one, called the Pantheon, is a representation of the Universe . Most historians estimate that they were built between the 3rd and 2nd centuries BC, but there are also other calculations (in relation to the summer solstice day), which indicate that they are even 600 years older. The most important (and the best known) of them are the great circular sanctuary, the Pantheon, and the andesite Sun. The andesite Sun sanctuary was dedicated to the worshipping of the Sun (Fig.4). It represents an undoubtable proof that the Get-Dacians worshipped the cult of the Sun, practiced the sacred fire and incineration as homages to the Sun. It is made up of a central disk consisting of 11 blocks perfectly combined, with a diameter of 7 meters, that continues with ten rays encrusted on the surface (each 2.76m long), of trapezoidal form, with the exterior sides forming a circle arch. To the North the disk is completed by an alley made of andesitic blocks that narrow away from the disk. This sanctuary resembles the circular one at Stonehenge, *i.e.* it functions as a sacred circle used for many kinds of magical practices, as well as a form of protection of the space where a ritual is carried out. There are also obvious similitudes between Stonehenge and this sanctuary. They have the same exact

North-South and East-West orientations and their alignment allows the solar rays to cross the inside from one end to the other, only during one day of the year, namely on 22 December, when the Suns declination is maximal and astronomical winter starts. In all zones where the Sun and the Moon were worshipped, that day was marked by fire ceremonies, whose goal was that the Sun should not "freeze" or disappear. The sanctuary is made of andesitic plates and is the place where the Sun was worshipped and sacrifices were brought to it. The Pantheon (Fig.4) is devoted to the whole cosmos.It is made up of three concentric circles and an arch with Hestias hearth in the middle of the arch. The arch stands for the Earth, while the circle next to it is that of the Moon, followed by the circles of the Sun and (moving stars), *i.e.* planets and last by that of the fixed stars.The two big gates are oriented to the solstices directions, the Men Gate corresponding to the summer solstice (Cancer astrological sign) and the Gods Gate corresponding to the winter solstice (Capricorn sign). This sanctuary was also used as a calendar. The arrangement of the pillars and blocks of stones in concentric circles leads to the conclusion that the Dacians knew the calendar of 365 days and the motion of the Sun throughout the year. The Dacians created a quite precise solar calendar, which they used especially in agriculture. Their solar calendar was considered the most precise one in antiquity. The Dacian monks also placed a sacred hearth of fire at the centre of their smaller, round, multi-circled sanctuaries raised in the area nearby Sarmizegetusa, and also made incinerations as homages brought to the Sun.

Circular altars dedicated to the Sun were discovered at Sărata Monteoru and Sighişoara (in Transylvania country) dating from the same Bronze Age.

Fig. 4 – The Andesite Sun and the Pantheon sanctuary at Sarmizegetusa.

Most probably the name given by the Dacians to the Sun was "Dzio". Hence come the present words "ziua" (day) and "zeu" (god), that has a close relative in

Italian, namely "dio".

With the Dacians everything started from the Sun. They considered that the New Year began on the date of the spring equinox, in March, when the Sun regained its powers and helped Nature revive. In March, when the Sun grew stronger, the Dacians resumed all activities: the agricultural works, the climbing of the sheep in the mountains for grazing, mining and the training of the armies. The solar cult continued in Dacia even after it was conquered by the Romans, in the 1st century AD. The Romans, too, had the old Persian cult of the god of light, Mithras that had spread rapidly in the Roman Empire, starting from the 2nd century until de 5th century AD. The Roman army had turned this cult into the cult of Sol Invictus (the unconquered Sun), that reached its climax during the reign of Emperor Aurelian, who raised a temple for it in 274 (*i.e.* three years after the withdrawal of the Roman troops from Dacia).

The Neolithic populations, especially the ancient Pelasgian current, people whose public and private lives were based on religion, had at the same time a special cult for the deceased. One of the most important Neolithic necropolis in Europe was discovered at Cernica, near Bucharest, the present capital of Romania. The majority of the tombs (96.3%) can be considered to have a solar orientation, corresponding to the Sun's azimuth at sunrise (Sîngeorzan, 1976). The measurement of the azimuth coordinate of the Sun at the summer solstice gives the median axe orientation of the tombs. It seems that the funeral rituals took place in the morning and that the bodies were placed in the tombs facing the Sun. This practice of burying the dead facing East was transformed to the orientation of the bodies with the head pointing Est with the Christian people.

3. THE CHRISTIAN CONTINUATION

Christianity, in general, and Romanian Christianity in particular, took over almost all dogmas and rituals of the religion of Mithras, the solar god, such as the celebration of the day of Sunday, Christmas, baptizement and the sacrament. The head cover of the Orthodox priests is called even today "mitra" and is taken over also from the Persian priests of Mithra. The birth of the Persian god Mithras, "The Sun of Rightness" was celebrated on the 25 of December, date taken over by Christianity for the birth of the Savior Jesus Christ.

The Sun has a special significance also in the Romanian folk culture. Actually, Romanian Christian religion also abounds in solar symbols and beliefs adopted from the pagan period, that overlapped and mixed up with the Christian beliefs. The old folk people speak even today of the Sun as Gods Star, Gods Eye, the Holy Sun, which, when it rises, makes all stars disappear. The Romanian Orthodox churches

are known for their pictures where cosmic aspects are often mixed with saint figures and biblical scenes. The Sun occupies an important position in this context - Fig.5 displays some examples.

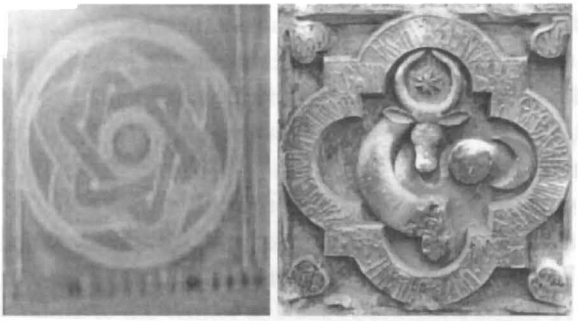

Fig. 5 – An wall picture at Voroneţ Monastery (left); coat of Arms of Moldavia, dating from the XVIth century found at Probota Monastery.

An important solar symbol in ancient times seemed to be the Cross sign. The specific Dacian cross is characteristically made up of a circle around the cross sign. Later it was made up of a circle inscribed with a cross or of a cross over passing its margins. The Orthodox cross contains the Sun rays and the Orthodox churches are recognized by their specific spiers, as Fig.6 displays.

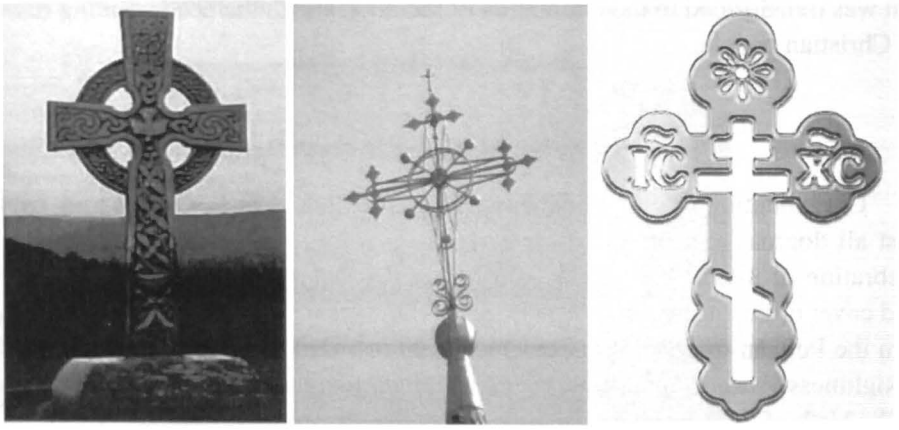

Fig. 6 – The Orthodox Cross, a mixture between a simple cross and the Sun symbol.

A remarkable thing in the architecture of the Christian churches orientation is the same concern for the Sun rise point. From the beginning, the Christian churches have been built with the altar facing the East, actually the point where the Sun rises

to spread light on the Earth. Tombstones are also facing the same direction.

4. SOLAR CULT TRACES IN THE ROMANIAN POPULAR ART

The Sun is present in the Romanian peoples outlook, starting with the Southward orientation of the folk houses, namely of the "prispa" (open verandas) or of the "foişor" (belvedere). The icons, the churches, the church altars and tombs always face the East. The older they are, the more deliberately they seem to observe the direction of the solstice sunrises. In the Romanian tradition the most frequent solar symbols are the sun wheel, the circle, the wheel with the cross in it, the mill wheel or the rhombus. These symbols are to be found also in the architecture of the folk houses. In many regions of Romania, such as in Bucovina, Maramureş, Oltenia, the Sun is carved on the pillars, doors and beams of the houses, being considered a good luck omen and a sign of protection against evil. Solar symbols are present also on the houses in Transylvania, Oltenia, as well as on the engravings of the churches in Maramureş.

The Romanian folk people have preserved till today the custom of carving many of the above mentioned solar symbols on various household objects such as dowry cases, distaffs, funeral stones, tools, pottery. Solar, along with lunar symbols can be found even on folk clothes in some parts of our country, such as on sheepskin sleeveless jackets in Bunila and Poienita Voinii, Hunedoara County, Transylvania. The most common Romanian folk custom related to the Sun is the trinket ("mărţişor"), which is actually a symbol of the spring Sun.

A famous Romanian tradition is represented by the Easter eggs painting. The Sun, stylised or not, occupies a central place in this painting, together with many geometric designs (Fig.7).

The worshipping of the Sun can be found also in some Romanian folk dances. The best example is "hora", which through its round shape imitates the roundness of the Sun. The origins of the "hora" dance come from the period when on the territory of our country dominated the cult of the Sun. At Bodeşti-Frumuşica was discovered a ceramics vase representing such a dance, namely a "hora" made up of six women. This object was dated as belonging to the Cucuteni Culture, approx. 3700-2500 BC. This is a clear proof that this traditional Romanian dance appeared more than 5000 years ago.

One of the most archaic agro-solar traditions in Romania is the dance of the *Caluşari* (Fig.8), a tradition practiced for 9 days,that begins (with the dance of the sunrise, around a mound) exclusively on the Whitsun. The dance, regarded as holy, is performed by 9 characters:"Vătaful" (king and pontiff), carrying a white flag, club, sword, etc, "Ceauşul" (with hammer, knapsack with 9 simples such as garlic, worm-

Fig. 7 – Easter eggs and a Maramureş region gate.

Fig. 8 – The traditional Romanian dance *Căluşarii* (it means the horsemen), a Sun worship ritual.

wood, etc) and 7 "caluşari" (who represent the solar horses of Apollo, in 9 dances, with jingle bells, clubs, etc), beside 2 bagpipe players and the "Mut", a dumb person with a whip. This tradition, marked also by the number 9, represents the prehistorical farmers invocation to the Sun, for the favoring and and protection of the harvests against the malevolent actions of the 9 fairies called "Rusalii".

In time, many Romanian rulers and princes, from all regions of our country, adopted symbols of the Sun in their coasts of arms or seals. We notice here a couple

of examples:

- the royal seal of Prince Stephen Stefan the Great, ruler of Moldavia, 15th century;
- the coat of arms of the Brancoveni royal family, rulers of Wallachia, 17th century;
- the coat of arms of the united Romanian principalities carried out by Prince Michael the Brave, the end of 16th century.

The symbol of the Sun is present in the present arms of Romania.

5. CONCLUSIONS

The Sun has fascinated the ancient inhabitants from many countries and continents, the inhabitants of the land between the Charpatian Mountains and Black Sea, our forefathers, included. In the Romanian tradition, the worshipping of the Sun has its roots in the Dacian prehistory and even much more in the old pre-Greeks and Thracians epochs, especially in the Pelasgian culture. Apollo, the God of the Sun, represented as a rider knight, the divination of Mithras and the Roman worshipping of Sol Invictus, were also widely spread in the Romanian ancient territories. The pagan symbols of the solar cult, Dacian and Roman alike, found their way into the daily life of the people, into their religion, art and folklore.

The ancient solar cult imbued even the Christian religion, influencing the orientation of the churches, icons and tombs, as well as the essence of the Orthodox cross. The Romanian folklore is rich in solar symbols, that are often used in the ornamentation of the folk household objects, clothes and houses Traditional solar symbols are to be found also on painted eggs and dances. The Romanian princes used the image of the Sun in their coasts of arms as a sign of dignity and power.

We can conclude that the day star of our planet, the Sun has been present with the inhabitants of the Romanian country places from Neolithic Age until the present day. This cult is very well integrated in the popular traditions, as well as in the Christian Orthodox religion.

REFERENCES

Bhatnagar, A., Livingston, W.: 2005, *Fundamentals of solar astronomy*, World Scientific Series in Astronomy and Astrophysics, Vol. 6

Crişan, I. H.: 2008, *Civilizatia geto-dacilor*, vol.1-2, Ed. Dacica, Bucharest

Densuşianu, N.: 1913, *Dacia preistorică*, translated by Alexandra Ioana Furdui at http://www.pelasgians.org

Georgescu, M.: 2011, *Dacia lui Zamolxis, zeul celest*, Ed. Antet, Prahova
Nour, A.: 2009, *Cultul lui Zamolxis. Credinţe, rituri şi superstiţii geto-dace*, Ed. Antet, Prahova
Păun, S.: 1999, *Insemnele cerului*, Ed. Tehnica, Bucharest
Sîngeorzan, I. C. : 1976, *IXe Congrès de l'Union Internationale des Sciences Préhistoriques et Protohistoriques*, Nice, Résumés des Communications, 347
Strabo: 20 AD, *Geographica*, VII, 13
Wikipedia Enciclopedy, http://en.wikipedia.org/wiki/Swastika#Origin_hypotheses

Received on 23 September 2012

NOTICE TO AUTHORS

ROMANIAN ASTRONOMICAL JOURNAL (RoAJ) is a peer-review journal that appears twice a year since 1991, covering the fields of Extra-galactic astronomy, Cosmology, Stellar Astrophysics, Solar Physics, Helio-sphere, Space Sciences, Celestial Mechanics, Astrometry, and History of the Astronomy.

The manuscripts submitted by authors must contain original scientific contributions, be prepared in English using a latex editor and accompanying figures in jpg or eps format. The manuscripts (pdf, latex and figures files) should be submitted to `roaj@aira.astro.ro`.

The first page should contain: articles title (brief and informative), author(s) name(s) and affilliation(s), followed by an Abstract in English, and Keywords. The text should be clear and concise. The Abstract will clearly present the main conclusions of the work, in no more than 10–15 lines. *The fonts* to be used are: 11pt. for the normal text, 13pt. for the paper title, 9pt. for author(s) name(s) and affiliation(s), abstract, keywords, titles of chapters and paragraphs, figure captions, tables, running titles, and references. *Chapters and Paragraphs:* Papers, except short notes, should be divided into chapters, numbered by Arabic numerals. Chapters may be divided into paragraphs denoted by the number of the chapter and the number of the paragraph; each chapter and each paragraph should have a short descriptive title (e.g. 3.2. Results). *Formulae* have to be centered and numbered consecutively in Arabic numerals, included in parentheses, on the right-hand side of the manuscript. Tables should be numbered consecutively in Arabic numerals; they should be introduced in the text at their appropriate place. *Figures* and illustrations should be submitted separately, in eps or jpg format, having a high quality, in order to allow their reproduction without retouching. Any lettering should be large enough to be readable after the figure has been reduced in size for printing. Captions should be introduced in the text at their appropriate place. All figures should be numbered consecutively in Arabic numerals and referred to in the text (e.g. Fig. 2 or Figs. 2-5). Photographs should be included only if essential and should be enlarged enough to allow a clear reproduction.

References should be indicated in the text by the authors name and year of publication. They should be listed in alphabetical and chronological order at the end of the paper, as follows: name and initial(s) of the author(s), year of publication, suitable abbreviation of the journal (or title of the book and publisher), its volume and page(s). The natbib package is necessary in order to obtain the correct bibliography style of this journal.

Detailed instructions for the preparation of manuscripts and the RoAJ latex style can be found at the journal page: `http://www.astro.ro/~roaj`.

ROMANIAN
ASTRONOMICAL
JOURNAL

Vol. 22, No. 2, 2012

CONTENTS

ISSN 2285-3758
ISSN-L 1220-5168

Rom. Astron. J., Vol. 22, No. 2, p. 93–166, Bucharest, 2012